Universidade do Porto
FEUP Faculdade de Engenharia

U.PORTO
INSTITUTO DE CIÊNCIAS BIOMÉDICAS ABEL SALAZAR
UNIVERSIDADE DO PORTO

Integrated Master in Bioengineering
Major in Molecular Biotechnology

Development of a photo-triggerable nanoparticle for efficient intracellular delivery of siRNA

Sara Isabel Fernandes Pereira

up201400047@fe.up.pt

Dissertation for the fulfilment of requirements to obtain the degree of Master in Bioengineering – Major in Molecular Biotechnology

---

Supervisor in FEUP: Doctor Pedro Lopes Granja

Supervisor in Biocant – UC Biotech, CNC: Doctor Lino Ferreira

Co-supervisor in Biocant – UC Biotech, CNC: Doctor Adrián Jiménez-Balsa

Porto, October 2016

Acknowledgements

First, I wish to express my gratitude to Doctor Lino Ferreira, as group leader in the Biomaterials and stem cell-based therapeutics laboratory, for giving me the opportunity to work in a group of excellence at several levels, which allowed me to improve myself at a personal and professional skills. I also wish to thanks him for the availability of resources to carry out the experimental part of this project.

Still, I would like to thanks to Doctor Lino together with Doctor Pedro Granja, for all support and guidance throughout this work. Their encouragement and suggestions gave me confidence and were determinant in the accomplishment of this work.

My gratitude to Adrian for the strong support and availability for all that I needed during this project and also for guidance and corrections of the dissertation.

A very special and big thanks to Josephine Blersch, a PhD student in the lab, to follow me in my daily work, for all the time dispensed with me, availability and help in the performance of techniques necessary for this work. Her help and great effort to be present in the right moments were crucial to achieve a work with quality. I would also to thanks her to give me personal support, motivation and confidence that allowed me to overcome several obstacles in critical situations, during this project.

Thanks also to all the group for the good environment and good times out of the work, kindness and availability, specially to Sandra Pinto and Emanuel for scientific discussions that contributed to the progress of the project and a special thanks to Henrique who helped me in statistical treatment of results.

I am thankful for the financial support for the project in which this work is enclosed, provided by research grant ERC project nº 307384, “Nanotrigger” from European Comission (EC).

Thanks to my friends who have accompanied me and people who crossed me over these years and that somehow contributed to my coming here, giving me personal and professional support.

A very special thanks to my parents, sister, my grandparents and my boyfriend for the encouragement, patient, support and endless love, that were very important for me to accomplish this stage of my life.

Thank you for all!!

"Twenty years from now you will be more disappointed by the things that you didn't do than by the ones you did do. So throw off the bowlines. Sail away from the safe harbor. Catch the trade winds in your sails. Explore. Dream. Discover."

H. Jackson Brown Jr., P.S. I Love You

- This page was intentionally left blank –

Abstract

siRNA-based therapies are very promising in diseases for which conventional therapies have no efficient effect. Despite the advances in the last years, the development of systems for the efficient intracellular delivery of siRNA is still of utmost need in particular for in vivo delivery. The current work aims to develop a photo-activatable nanoparticle formulation for efficient delivery of siRNA within cells. Nanoparticles were prepared by the nanoprecipitation of a poly (amido amine)-based polymer bearing a pendant photo-cleavable moiety responding to ≈355 nm wavelength exposure. Two types of nanoparticles were obtained: C11 nanoparticles, from non-purified polymer, and C11_P nanoparticles, from the purified polymer. Our results show that the NPs had an average size of 117.7±0.2 nm and 61.2±0.06 and a zeta potential of 22.7±1.15 and 15.2±1.27 mV, respectively for C11 and C11_P nanoparticles. Both nanoparticles were then complexed with siRNA. The slightest changes shown in zeta potential values of C11 nanoparticles indicate that these nanoparticles have higher ability to compensate siRNA negative charges, comparing to C11_P nanoparticles. The light-triggerable properties of the nanoparticles were evaluated after exposure to UV (365 nm, power of 100 mW/cm^2) or a blue laser (405 nm, power of 100 mW/cm^2). The number of nanoparticles was then estimated from Kcps values of complexed nanoparticles before and after activation obtained from DLS measurements. Our results showed an efficient photo-disassembly of C11 nanoparticles after light activation (57% after UV, 365 nm, 100 mW/cm^2, 10 minutes; and 89% after laser, 405 nm, 100 mW/cm^2, 10 minutes). In the same activation conditions, the photo-disassembly process of C11_P nanoparticles was lower than C11, perhaps due to the loss of short molecular weight polymers with an important role in C11 nanoparticles photo-responsiveness. UV/vis spectrophotometry analyses further confirm these results, showing an increase of free DMNC moieties in C11 nanoparticles supernatant after light activation. The cytotoxicity and siRNA delivery properties of C11 and C11_P nanoparticles were evaluated in a HeLa-GFP reporter cell line. C11 nanoparticle showed low cytotoxic in cells up to a concentration of 20 μg/mL, before or after UV light activation (365 nm, 1 mW/cm^2, up to 10 minutes) or blue laser irradiation (405 nm, 20 and 10 mW/cm^2, up to 3 minutes). GFP knockdown results showed that siRNA release mediated by photo-activatable C11 nanoparticles is photo-triggered by UV light (365 nm, 1 mW/cm^2) after exposure for 10 minutes and by blue laser (405nm, 10 mW/cm^2), after 30 second of exposure. Moreover, results showed that siRNA intracellular release mediated by photo-activatable C11 nanoparticles is even more efficient than siRNA release using lipofectamine. Overall, our results show that C11 nanoparticles are promising formulations for the intracellular delivery of siRNA. Our results show that the use of a blue laser may be advantageous relatively to UV light because allows siRNA release from NPs in a short period of time without compromising cell viability. The results described in this thesis pave the way for the development of new synthetic vectors for the intracellular delivery of non-coding RNAs with spatio-temporal control.

- This page was intentionally left blank –

Table of Contents

List of Figures

List of Tables

- This page was intentionally left blank –

Abbreviations and Symbols

Ago2	Argonaute 2 protein
APEG-DOX	Polyacetal-based nanoparticles conjugated with doxorubicin
Asp	Aspartate
BCP	Block copolymer
C11	Referent to non-purified polymer
C11@siRNA	C11 nanoparticles complexed with siRNA
C11_P	Referent to purified polymer
C11_P@siRNA	C11_P nanoparticles complexed with siRNA
C_{18}	Carbon 18
CY5	Cyanine far-red-fluorescent dye
DLS	Dynamic light scattering
DMEM	Dulbecco's modified eagle medium
DMNC	4,5-dimethoxy-2-nitrobenzyl chloroformate
DNA	Deoxyribonucleic acid
DOPE	1,2-dioleoyl-*sn*-glycero-3-phosphoetanolaine
DOX	Doxorubicin
dsRNA	Double strand ribonucleic acid
EDTA	Ethylenediaminetetraacetic acid
EPR	Enhanced permeability and retention effect
FBS	Foetal bovine serum
FEUP	Faculdade de Engenharia da Universidade do Porto
GFP	Green fluorescence protein
Glu	Glutamine
H33342	Hoechst 33342
HCl	Hydrochloric acid
ICBAS	Instituto de Ciências Biomédicas Abel Salazar
Kcps	Kilocounting per second
KO	Knockdown
LCST	Low critical solubility temperature
lncRNA	Long non-coding ribonucleic acid
Lys	Lysin

miRNA	Micro ribonucleic acid
MNP	Magnetic nanoparticles
mRNA	Messenger ribonucleic acid
n	Population size
ncRNA	Non-coding ribonucleic acid
NIR	Near-infrared
NP	Nanoparticles
NP@siRNA	Nanoparticles complexed with siRNA
ODN	Exogenous oligonucleotides
O-NB	*O*-nitrobenzyl
PALS	Phase analysis light scattering
PAMAM	Poly(amido amine)
PBS	Phosphate buffered saline
PEG	Polyethylene glycol
PEI	Polyethylenimine
Pen	Penicillin
PEO	Poly(ethylene oxide)
pH	Potential of hidrogen
PI	Propidium iodide
piRNA	Piwi ribonucleic acid
PLGA	Poly lactic-*co*-glycolic acid
PMA	Poly(methacrylate)
PNBC-*b*-PEO	Poly(s-(*o*-nitrobenzyl)-L-cysteine)-*b*-poly (ethylene glycol)
PNIPAM	Poly(n-isopropylacrylamide)
QeLS	Quasi-elastic light scattering
RISC	RNA-induced silencing complex
RNA	Ribonucleic acid
RNAi	Ribonucleic acid interference
SEM	Standard error of the Mean
SFE	Semi-continuous flow electroporation
siRNA	Short interference ribonucleic acid
sncRNA	Small noncoding ribonucleic acid
SPIONS	Superparamagnetic iron oxide nanoparticles

Strep	Streptomycin
UV	Ultraviolet
Vis	Visible
λ	Wavelength

%	Percentage
µg	Microgram
µl	Microliter
cm	Centimeter
cm^2	Square centimeter
G	G-force
h	Hour
KHz	KiloHertz
mg	Milligram
min	Minute
mL	Millilitre
mM	Milimolar
mV	miliVolt
mW	miliWatt
nm	nanometer
ºC	Celsius degree
rpm	Revolutions per minute
V	Volt
W	Watt

- This page was intentionally left blank –

Chapter 1: Thesis structure and goals

Despite the significant progresses done during the last years in the intracellular delivery of siRNA, efficient systems are still missing. This is because our understanding about nanoparticle cellular uptake and intracellular trafficking is still very poor. On the other hand, the development of nanocarriers with properties (composition, structure, physicochemical properties, surface chemistry and target ability) that make them able to complex siRNA and, at the same time, overcome all barriers associated with siRNA delivery and improve its cellular uptake is still needed.

The general aim of this project is to develop a photo-triggerable nanoparticle for the efficient transfection and delivery of siRNA. The project took advantage of polymeric nanoparticles previously identified in Lino Ferreira lab called C11 nanoparticles. C11 nanoparticles have in their constitution a poly (amido amine)-based polymer and a pendant photochromic moiety 4,5-dimethoxy-2-nitrobenzyl chloroformate (DMNC), which have, a photo-cleavable O-nitrobenzyl (*O*-NB) modified group (Figure 1).

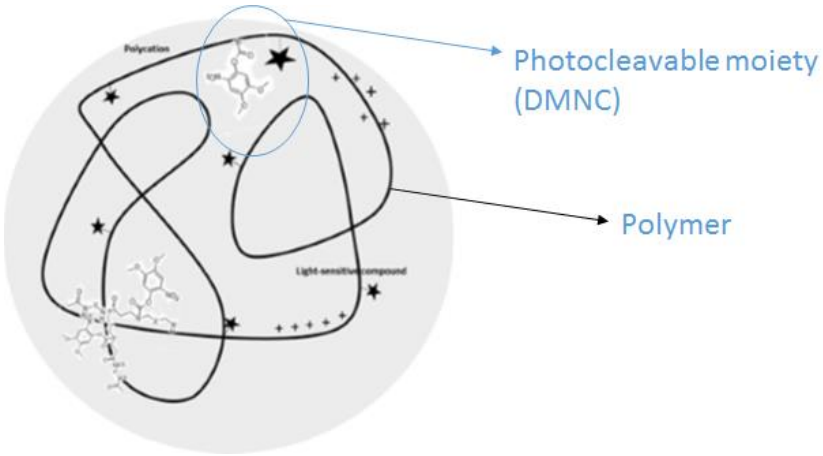

Figure 1. Schematic representation of developed poly (amidoamine)-based nanoparticles, with pendant photo-cleavable moieties of 4,5-dimethoxy-2-nitrobenzoate.

The present work was divided in two phases:

1) The first phase comprised the review of the literature about photo-triggerable nanoparticles and siRNA delivery, and the elaboration of a work plan. This phase did occur during the first semester of the 2015/2016 academic year.
2) The second phase comprised the experimental work and did occur during the second semester (February until July, academic year 2015/2016).

Regarding the experimental work, the first task was the production and characterization of C11 nanoparticles, using non-purified and purified poly (amido amine)-based polymer. Nanoparticles were produced by nanoprecipitation and characterized by size and zeta potential analyses before and after complexation with siRNA. Then, the effect of UV and blue

laser light in size and zeta potential was assessed. Still in this step, nanoparticles photo-responsiveness was observed in a first assay, by Kcps count decrease of nanoparticles after light exposure. The next step was to confirm the disassembly of nanoparticles by a blue laser, observing if the quantum yield of irradiation source was enough for the disassembly of our nanoparticles.

The ensuing task was to perform *in vitro* assays, using HeLa-GFP reporter cell line. The aim was to study the bioactivity of the photo-responsive nanoparticles in transfected cells. Here, the first step was to establish the optimal light conditions to photo-activate the nanoparticles and, at the same time, to avoid photo-cytotoxicity. Then, using established light conditions, the cytotoxicity of photo-activated nanoparticles was assessed by cell viability determination and the intracellular siRNA release mediated by nanoparticles was assessed by GFP knockdown (GFP KO).

The current thesis is divided in 4 chapters. Chapter 1 presents the project motivation, main goals of the work and the general structure of the dissertation. Chapters 2 reviews the literature about the relevant points of the current work including description of the main developments and the main challenges in the field, providing a theoretical basis. Chapter 3 includes the list of main materials used for the experimental part, as well as the methodologies used. Chapter 4 presents and discusses the main experimental results in the setting of the literature. There are also included the main conclusions, achievements during the current work and suggestions for additional work. Finally, the dissertation includes also a section with supplementary material for additional information.

- This page was intentionally left blank –

Chapter 2: Introduction

How drugs are delivered into biological systems is extremely important, since it influences the ability or not of a drug to reach and act efficiently in one specific site (organ, tissue or cell). The major challenges associated to the drug delivery are related to the pharmacokinetic and pharmacodynamic characteristics of the drug. Given the inefficiency of the traditional drug delivery systems, the development of vehicles able to carry drugs and direct them towards to a specific site of action is need. The main requirements of these drug carriers are: (a) ensuring drugs properties are not compromised during their transport and (b) improving drug therapeutic effect in those sites where they need to act [1].

Several drug carriers have been developed in the last years to increase the intracellular delivery of biomolecules such as microparticles and nanoparticles [2]. This drug carriers vary in size, shape and composition. In case of microparticles, they load a large amount of drug and so multiple drug doses can be released in a single administration. However, due to the risk of embolic processes, nanoparticles are more indicated for systemic administration. Nevertheless, these carriers can be easily degraded under specific conditions, and thus delivering a massive amount of drug that can be harmful for the organism [3]. Yet, as it will be explained in next sections, the use of nanoparticles has several advantages over microparticles for intracellular delivery of non-coding RNAs.

1. Non-coding-RNAs: lncRNA, sncRNA

Drugs (pharmacological substances that treat or prevent a disease) can be administrated in the body orally, through the respiratory tract, skin or directly injected in the bloodstream, depending on the organ, tissue or cells to be treated and the type of action that is intended (topical or systemic). RNA molecules, especially non-coding RNAs (ncRNA), are very promising therapies to treat diseases where traditional pharmacological molecules fail [4, 5]. Non-coding-RNAs are RNA molecules which are not translated in proteins but modulate mRNA translation (Figure 2). Since the discovery of the first ncRNA (60 years ago), a large number of these molecules have been founded and related with biological functions.

In general, ncRNA can be divided in two main groups: long non-coding RNA (lncRNA), which have sequences with more than 200 nucleotides, and short non-coding RNA (sncRNA), which comprise shorter sequences of less than 30 nucleotides [6]. sncRNA are the most relevant in gene expression control and have been shown as the most promising for therapeutic applications. The main classes of sncRNA known until now are piwiRNA (piRNA), microRNA (miRNA) and short interfering RNA (siRNA). They differ from each other in the sequence length and, more importantly, in the way that each one act to control gene expression.

In this work, we have selected siRNA to modulate cell activity. First, the effect of siRNAs is much more quantifiable than other non-coding RNAs such as miRNAs. Second, siRNA molecules are closer to the market than other non-coding RNAs. Therefore, the advantages of siRNA usage and its high potential as therapeutic agent will be explored in next sections.

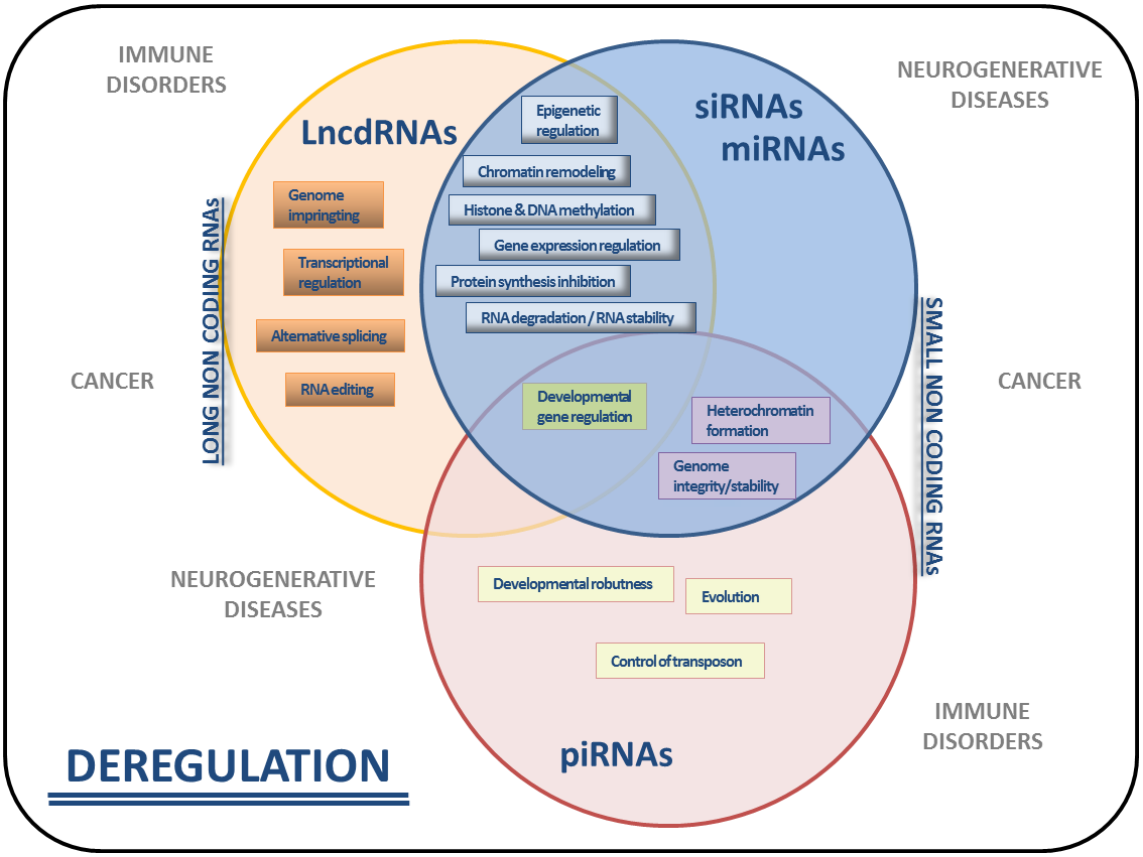

Figure 2. Scheme showing the biological role of non-coding RNA (ncRNA) molecules. Deregulation of specific long non-coding RNA (LncRNA) or small non-coding RNA (siRNA, miRNA or piRNA) expression leads to gene defective disorders, described outside of the circles. Adapted from [6].

1.1. siRNA: mechanism

siRNA are small fragments of RNA sequences with roughly 20-25 nucleotides [7]. These molecules have a role in the control of gene expression at a post-transcriptional level, and so have a role in biological functions by controlling protein expression (full inhibition or partial activity decrease). siRNA acts using a specific internal mechanism of gene silencing, called RNA interference (RNAi). In general, iRNA mechanism involves 3 main steps (Figure 3) [8]:

1. **Long double stranded RNA (dsRNA) cleavage:** dsRNA transcripted in the nucleus are cleaved in the cytosol, by a specific enzyme ribonuclease (RNase) III-like, called DICER. As result, small dsRNA with roughly 21-23 nucleotides are formed.
2. **RISC complex activation:** small dsRNA interacts with RNA-induced silencing complex (RISC) and is dehybridized in siRNA sense strand and siRNA antisense strand. The siRNA

antisense strand binds to AGO2, a specific catalytic molecule belonged to Argonaute family, that are present in RISC complex. Once bounded with siRNA strand, AGO2 becomes active and able to recognize specific mRNA sequences for gene silencing process.

3. **Target mRNA recognition and specific gene silencing**: the activated RISC complex-siRNA recognizes, by complementarity of nucleotides, specific sequences of mRNA, cleaves and degrade targeted mRNA and so genes appertaining to these mRNA sequence are knockdown or silenced.

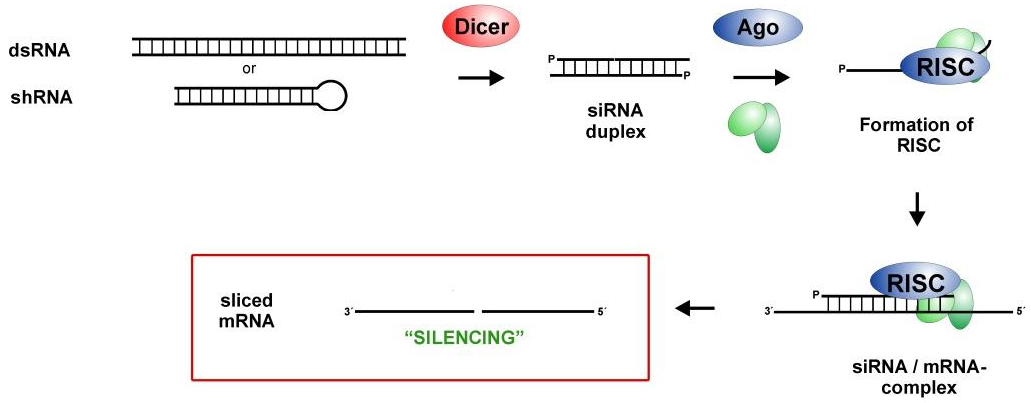

Figure 3. Interference RNA (iRNA) mechanism and siRNA gene silencing. Adapted from http://www.uni-konstanz.de/FuF/chemie/jhartig/, accessed on 7th February 2016.

Nowadays, the siRNA commonly used in biomedical applications is produced exogenously in the laboratory for it to be delivered into the cell cytoplasm, so DICER action is no longer necessary in these cases. All the remaining processes occur in the same manner as in the endogenous iRNA mechanism.

1.2. siRNA in gene therapy

Gene therapy refers to methods for transferring genetic material (nucleic acids, such as DNA or RNA) into specific cells. Gene therapy is an alternative method to treat, prevent and/or control diseases for which traditional therapies do not show yet the expected therapeutic effect [9]. As mentioned above, the ability of siRNA to target specific RNA sequences and consequently control specific pathological proteins already overexpressed or in risk to be overexpressed, gives to siRNA a high potential to treat specific genetic diseases caused by upregulated proteins. In this context, thanks to its ability to improve effective therapeutic effect, siRNA have shown a high potential in gene-based targeted therapies [10, 11].

siRNA molecules are currently being evaluated in cancer treatment, as some siRNAs can control cells proliferation and induce apoptotic events in tumor cells [10]. In addition, siRNA molecules are being evaluated in the treatment of Alzheimer's [10], macular degeneration [12], genetic disorders [12] and psoriasis [13]. Finally, siRNA is a useful tool to control the differentiation and proliferation of stem cells and thus has a high potential in Regenerative Medicine and Tissue Engineering areas [14, 15].

1.3. siRNA delivery: viral *versus* non-viral strategies

Exogenous nucleic acids such as siRNA can be delivered directly into the cells using two different transfection methods: viral and non-viral [8]. Viral-based strategies where the first to be developed and consist in the use of viruses as carriers for nucleic acids, after the virulence genes have been removed from viruses' DNA. Despite the high efficiency of gene transfection, these methods present several drawbacks such as immunogenicity, high probability to trigger oncogenes expression and difficulty to scale up the manufacturing process. Non-viral strategies have been developed in order to overcome the limitations of viral-based strategies. These strategies comprise the development of molecules which are biocompatible, non-toxic, non-immunogenic and are not integrated into the hosted genome. In addition, these strategies are advantageous since manufacturing process is easily reproduced and more simply controlled than viral transfection processes. One of the fewer disadvantageous is the lower rate of transfection efficiency compare to viral strategies. In this sense, several approaches have been developed in order to improve the efficiency of non-viral carriers for nucleic acids delivery. Among the various non-viral approaches, nanoparticles are specially highlighted since its high potential as nucleic acid carriers is well described in the literature [16].

2. Nanoparticles for drug delivery

Nanoparticles are promising formulations for several biomedical applications. On one hand, nanoparticles may protect the drug from potential degradation by environmental factors, maintaining their original properties and stability. On the other hand, nanoparticles may also improve pharmacokinetic and pharmacodynamic properties (administration, distribution, metabolism and elimination), and thus improve therapeutic efficacy of the drug [17].

Physicochemical properties of the nanoparticles have a key role in the successful development of nanosystems for drug delivery. Thus, when nanoformulations are produced, parameters such as size, composition and surface charge must be taken into account [17]. Nanoparticle size plays a key role in nanoparticles biodistribution and, in case of intravenous administration, it is an important parameter to control nanoparticle circulation time in the bloodstream [18]. In addition, it is important to control the size distribution of the

nanoparticles to obtain homogenous colloidal suspensions. The size is highly related with the surface charge of nanoparticles and so, controlling the size is important for nanoparticles stability [19].

Nanoparticles with a size less than 10 nm have a rapid clearance and are quickly eliminated through the liver and kidneys. However, nanoparticles with size larger than 200 nm (a) are easily phagocyte and (b) have more difficulty to cross biological membranes [19]. Thereby, for efficient drug delivery, nanoparticles must ideally have a size in a range between 100-200 nm in order to improve cellular uptake and nanoparticles internalization [19-21].

Nanoparticle surface/volume ratio plays also an important role in drug delivery. In contrast with larger particles, nanoparticles have a large surface area compare to their volume. The large surface area increases the interaction between the payload and the nanoparticle, making the drug complexation and entrapment more efficient.

Nanoparticle charge is also very important in drug delivery. Nanoparticle charge is measured by the zeta potential. Nanoparticles having a high zeta potential are less likely to aggregate and are more stable as a colloidal suspension [22]. The ideal surface charge of nanoparticles depends strongly on the characteristics of drugs that are intended to encapsulate or complex. For example, if the objective is to complex or encapsulate drugs negatively charged such as nucleic acids, nanoparticles with high positive charge are more advantageous since the drug complexation is more efficiently.

Additionally, biological membranes have in general negative potential. Thus, particles with high positive surface charge can interact better with cells membrane. Since the charge of cells membrane may vary depending on the type of tissue, by controlling the surface charge of nanoparticles it might be possible to improve cell uptake and internalization. In addition, nanoparticles with high positive charge can aggregate more easily with blood proteins, are highly cytotoxic and immunogenic [19].

Several nanoparticle surface modification strategies are often applied to improve nanoparticle physical and chemical properties, aiming to minimize opsonisation and prolong circulation of nanoparticles *in vivo*. As example, nanoparticle surface can be modified with hydrophilic surfactants such as polyethylene glycol (PEG) and polysorbate 80 (Tween®80), which results in an increase of nanoparticles time circulation in blood and decrease of nanoparticle phagocytosis [19].

As was mentioned in previous sections, targeted drug delivery aims to direct nanoparticles to target cells, tissues or organs. Targeting allows the accumulation of drug in specific sites in therapeutic concentrations and as consequence, decrease the frequency of drug administration and toxic side effects on untargeted cells [19]. In targeted delivery strategies, two main approaches can be considered: active target and passive target (Figure 4) [23]. In active target approaches there is a functionalization of nanoparticles surface with specific ligands to enhance the delivery of nanoparticles into targeted sites. Targeted cells can express receptors in their surface, which are able to recognize specific molecules (e.g.

antibodies, aptamers, peptides or sugars). Thus, it is possible to functionalize nanoparticles with these molecules, and so, recognition and interaction between nanoparticles-targeted cells is improved. Passive target is based in making use of the physicochemical properties of nanoparticles (size, charge and shape), so they can escape the body defense mechanisms (such as opsonization and phagocytosis), keep in circulation in the bloodstream and, by themselves, are taken in specific tissues. The specific accumulation of nanoparticles is related with specific properties of the target site. In other words, inside the body there are microenvironments, where are present specific physiological conditions (for example in terms of pH and temperature) which work as internal stimuli to take nanoparticles with favorable physicochemical properties, leading to the accumulation of nanoparticles in specific target sites. The nanoparticles can be accumulated in the environment surrounding cells or pass through the cells by diffusion or convection processes.

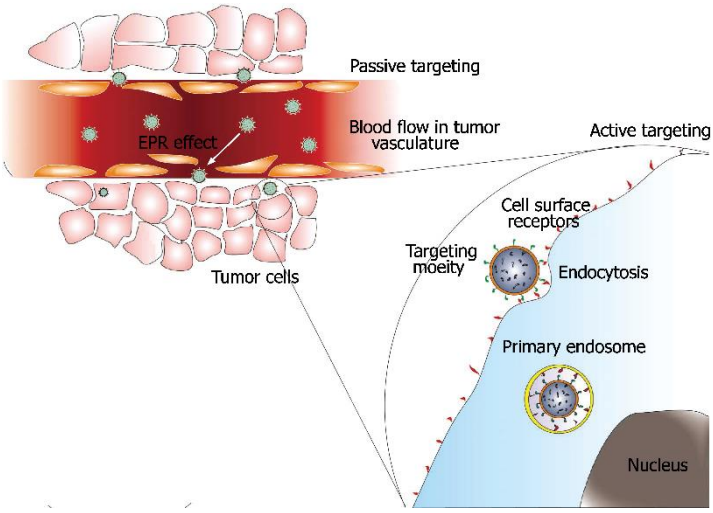

Figure 4. Illustration of the two types of target strategies. a) Passive target in tumor cells. Tumor cells have specific physical characteristics: pH lower than in healthy cells and more fenestrations between cells of endothelial blood vessels (leak blood vessels). Nanoparticles with specific size and sensitive to these pH conditions can be accumulated in the surrounding tumoral microenvironment (enhanced permeability effect – EPR) and enter in cells by diffusion or convection. b) Active target: nanoparticles with specific ligands are recognized by specific cells-receptors and enter in the cells by endocytosis pathways. Adapted from [23].

2.1. Types of nanoparticles

In general, nanoparticles can be inorganic (such as magnetic, gold nanoparticles, ceramics – e.g. with silica and titanium) or organic (such are liposomes, lipidic nanoparticles, polymeric nanoparticles and carbon-based nanoparticles – e.g. carbon nanotubes) (Figure 5) [24-27]. Organic nanoparticles, specifically liposomes and polymeric nanoparticles, have a great potential in drug delivery, because they can encapsulate both hydrophilic and hydrophobic drugs, and they are usually formed by biodegradable and biocompatible materials as building blocks. In addition, these nanoparticles can be easily functionalized and their composition readily modified, allowing the possibility to engineer nanoparticles in which

the delivery and payload release can be controlled and efficiently directed to specific target sites [28]. A good example of nanoparticles developed for controlled drug delivery and release are stimuli-responsive nanoparticles, which are described in the next section of this work.

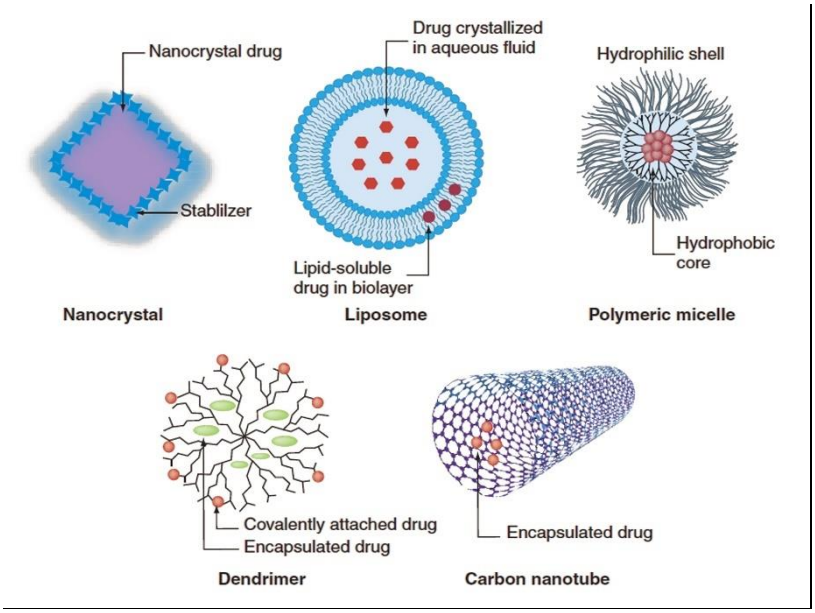

Figure 5. Examples of nanoparticles used as drug delivery systems. Adapted from [27].

2.2. Stimuli-responsive nanoparticles

Among the so called "smart materials" [29], the stimuli-responsive nanoparticles are one of the most interesting carriers used for drug delivery. These particles can release their payloads in specific sites, in a temporal controlled way. In the presence of a stimulus, changes on nanoparticles properties can occur. This can lead to nanoparticles destabilization and consequent increase of nanostructures permeability, or even to nanoparticles disintegration and therefore drugs inside or conjugated to nanoparticles are released in both cases.

Stimuli-responsive nanoparticles are one of the most promising strategies in drug delivery. These nanoparticles allow the release of the drug with spatio-temporal control. The release of the payload from the nanoparticles can be triggered only when a specific stimulus is present, stopping when the same stimulus ends, allowing an on-demand controlled release (temporal control). In general, there are two types of stimuli to which nanoparticles can respond: internal and external stimuli. Looking for an improved drug release, stimuli can be applied isolated or in a combined way, being possible to develop multiple stimuli-responsive nanosystems (Figure 6).

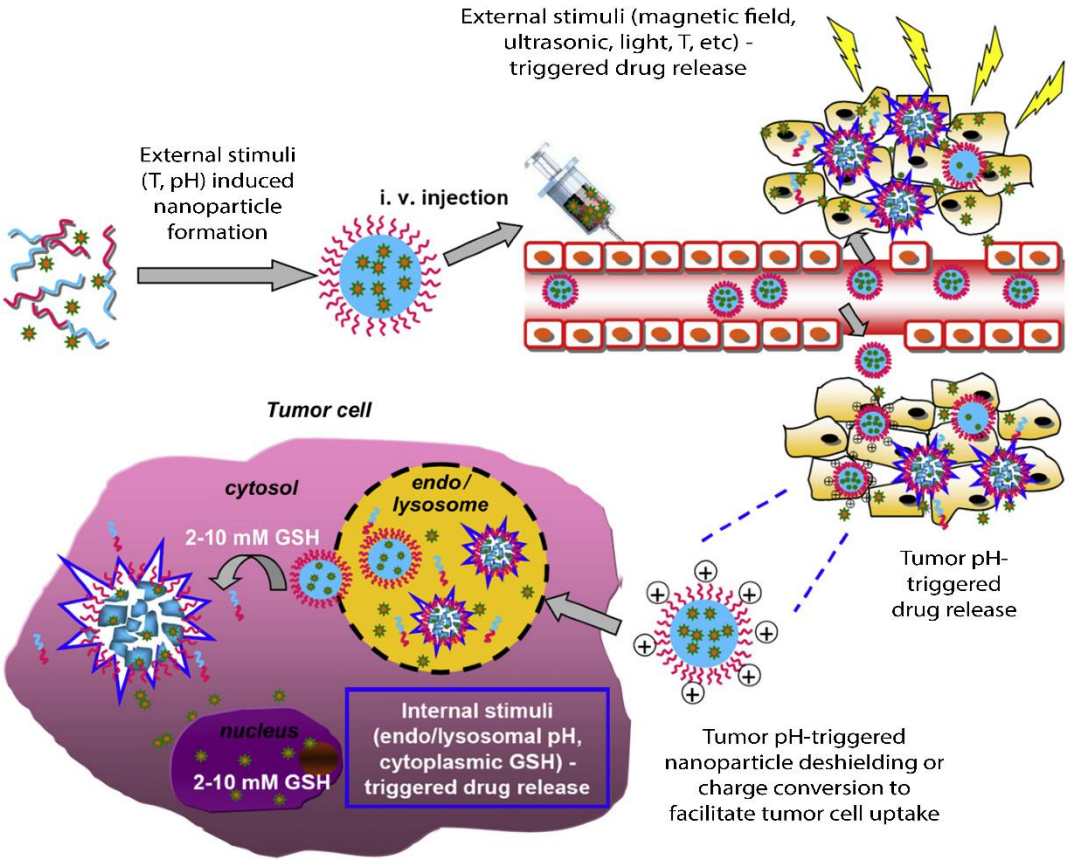

Figure 6. Multiple stimuli responsive nanoparticles developed to improve efficiency in cancer treatment. Adapted from [30].

2.2.1. Internal stimuli

In the body, there are specific environmental conditions which differ between organs or even intracellular compartments. Knowing the specific conditions, it is possible to design nanoparticles towards a particular site. Internal conditions such as pH, specific concentration (or activity) of enzymes, redox potential and temperature can act as stimuli, triggering a targeted controlled delivery of the nanoparticle payloads [31-35].

Nanoparticles may respond to specific pH's by alterations in their swelling/deswelling properties as well as surface charge leading to nanoparticle aggregation/disaggregation [32]. In biological systems, intracellular and extracellular pH can be affected by diseases such as cancer, but also other infectious or inflammatory diseases. pH-sensitive nanoparticles have been developed to selectively release anticancer drugs in tumour cells that have a lower microenvironmental pH than healthy cells [36]. This is very important since it avoids cytotoxicity of those drugs in healthy cells. For example, poly(acetyl-doxirubicin) nanoparticles conjugates (APEG-DOX) highly accumulate in cancer environments and, after pH-dependent degradation, DOX is released in tumour cells [37].

Nanoparticles may respond also to specific enzymes secreted in the context of a disease. It is possible to design nanocarriers that in the presence of specific enzymes, are degraded, and thus they release their payload. Two approaches can be followed. First, the nanoparticle

can be designed with enzyme-sensitive linkers that are degraded by specific enzymes allowing drug release from the nanoparticle. Second, the nanoparticle can be developed to incorporate moieties that are sensitive to the enzymatic cleavage leading to changes in the nanoparticle structure and subsequent drug release [32]. In this last case, we can include Opaxio™, a conjugate of PLGA-paclitaxel used to treat ovarian cancer. The ester linkage between PLGA polymer and the drug paclitaxel is cleaved in presence of a lysosomal enzyme (Catherin B), and so the drug is released [38].

Nanoparticles may also respond to redox potential found in the extracellular and intracellular environments. The extra- and intracellular environments have different redox potential related to glutathione levels. In an intracellular environment, glutathione concentration is higher than outside the cell and consequently, intracellular redox potential is lower. Since genes should be delivered in the intracellular environment, redox-sensitive polymers for gene delivery have been developed [39]. In this context, cationic polymers for DNA or siRNA delivery with disulphide cross-linkers have been described. Those linkages are cleaved due to lower intracellular redox potential and so genes are delivered within the cell [40].

Another example of nanoparticles that respond to internal stimuli are those sensitive to temperature. Thermo-sensitive nanoparticles can change their structure when temperature conditions are changed [41]. A typical example is the well-known thermos-sensitive polymer poly(N-isopropylacrylamide) (PNIPAAM), which normal lower critical solution temperature (LCST) is 31-32ºC. At temperatures above LCST, PNIPAAM structures are more hydrophilic in aqueous solution which leads to polymer solubilisation and consequently release of the payload. More importantly, the LCST of PNIPAAM can be rised until body temperature (37ºC) and thus the release of the drug at 37ºC or slightly above. Several nanoparticles having PNIPAAM have been developed, especially for the release of anticancer drugs such as paclitaxel. As example, PNIPAAM-based nanoparticles (LCST 37ºC) have been used for the delivery of paclitaxel under cancer temperature conditions (39.5ºC) [42].

2.2.2. External stimuli

External stimuli are exogenous triggers which, when applied to sensitive nanoparticles, promotes the release of their payload [32, 34]. Comparing with internal stimuli, external stimuli are more advantageous since allow the precise control of drug release in a remote way. Different nanoparticles have been designed for releasing their cargo only when the appropriate stimulus, for which they are sensitive, is applied. As triggers, several stimuli can be applied: magnetic field, electrical field, ultrasounds and light [32].

In some cases, the release from nanoparticles can be triggered by applying an external magnetic field. The main family of magnetic-sensitive nanoparticles are superparamagnetic iron oxide nanoparticles (SPIONS) which have in their composition materials with magnetic properties, such as magnetite (Fe_3O_4) or maghaemite (Fe_2O_3) [43-45]. Magnetic field can have

different effects. Kumar *et al* (2014) described SPIONS which, under an external magnetic field, overheat, leading to hyperthermia effect widely used in cancer therapy. In other cases, external magnetic field can trigger drug release from nanoparticles [45]. In their work, Chorny *et al* developed polylactide-based magnetic nanoparticles (MNP) encapsulating paclitaxel for treatment of in-stent restenosis, a pathology characterized by the reobstruction of arteries post stenting, and demonstrate that the drug efficiency can be increased in target sites. In this study, they used a magnetic targeting via uniform field-induced magnetization in polylactide-based MNP, which specificaly deliver paclitaxel in a rat carotid artery model. There, they shown that there was a significant increase of local concentration of their MNP in stent arteries, comparing to non-stented arteries, which leads to a significant inhibition of the pathology with relative low doses of paclitaxel.

Electrical fields can be used to promote drug release by diverse mechanisms of action. One example is the electroporation mechanism which is described as a highly efficient method for drug delivery. In this case, an electrical field with low voltage (typically 1V) is applied to get two different effects: 1) to form pores in biological membranes, increasing their permeability to drugs; 2) to enhance nanoparticles disintegration, triggering drug release [32]. It is especially useful for gene transfection or nucleic acid delivery against cancer [46]. As example, Wang and coworkers mixed transferrin-targeted liposomes complexed with exogenous oligonucleotides (ODN) with a chronic myeloid leukemic cell line and studied the effect of a semi-continuous flow electroporation (SFE) in ODN release itself and its consequent effect in leukemic cells. In their work, they observed that: 1) transferrin-ligand drives nanoparticles to leukemic cells, leading to its accumulation around the cell membrane; 2) when the SFE is applied to the cells, cell membranes became more permeable and an increase in ODN delivery was achieved.

The application of ultrasonic waves can trigger drug release by thermal or mechanical (cavitation phenomenon) effects. In both cases, by the application of ultrasonic low frequencies, there is an increase in cell permeability together with a rapid degradation of nanoparticles. The effect of ultrasounds has been evaluated in Pluoronic P105 micelles encapsulating DOX for the treatment of tumours. Low frequency (70 kHz and 1.5W/cm^2) ultrasounds are enough to trigger the release of DOX from Pluoronic P105-based micelles encapsulating DOX, resulting in a significant decrease of tumor volume [47].

In other cases, the release can be triggered by light. Light is one of the less invasive strategies to remotely control drug release [48, 49]. Nowadays, it is possible to synthesize several photo-activatable nanoparticles and trigger the release of their payload at a specific wavelength. These nanoparticles are sensitive to the specific wavelength, power and time of exposure of the light source. It is possible to apply a laser with a selective and precise spot, activating specific areas and so triggering the drug release in specific sites with high precision [50]. It should be noted that light might have some cytotoxicity depending on the wavelength, power and exposure time. Since these parameters are adjustable, it is in most cases possible to have photo-triggerable nanoparticles with a low toxicity [49, 51].

2.2.2.1. Ultraviolet (UV) light

UV radiation (wavelengths below 400 nm) is a high-energy radiation enough to break chemical bounds. Additionally, UV wavelengths have a low tissue penetration and so they can be mainly applied in superficial tissues, such skin and eyes (Figure 7) [32]. Moreover, UV light radiations are strongly absorbed by biological chromophores, such as hemoglobin, and are highly cytotoxic when applied for a long time [52]. In order to minimize the cytotoxic effects, when using UV radiation, it is necessary to take into account which wavelength will be applied, which light intensity will be used and during which time biological tissues will be exposed.

2.2.2.2. Near-infrared (NIR) light

NIR radiation (wavelengths between 650 and 900 nm) is a low energy radiation having a high tissue penetration (Figure 7) [51]. The low absorption of NIR radiation by biological chromophores makes them less toxic than UV light. Thus, NIR can be applied precisely and deeply into tissues without inducing a biological damage [52]. This is an important advantage that makes possible the application of NIR wavelengths to *in vivo* studies for clinical applications, for disease treatment (drug release) or in bioimaging (diagnosis) [53-55].

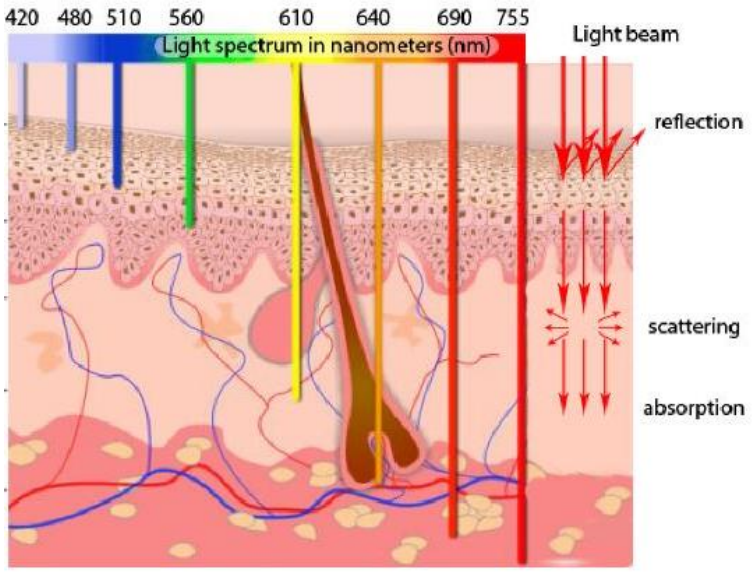

Figure 7. Schematic representation of tissue penetration depth of different wavelength of light. Adapted from http://reflexions.ulg.ac.be/cms/c_41432/fr/la-lumiere-contre-le-cancer?portal=j_55&printView=true, accessed on 26th January 2015.

3. Photo-activation mechanisms

Photo-sensitive nanomaterials can be photo-activated by mainly two different ways: physical-based principles or photochemical processes (Figure 8). Development of photo-sensitive nanoparticles would allow, after NPs uptake (and targeting), the triggered release of their payload in specific sites.

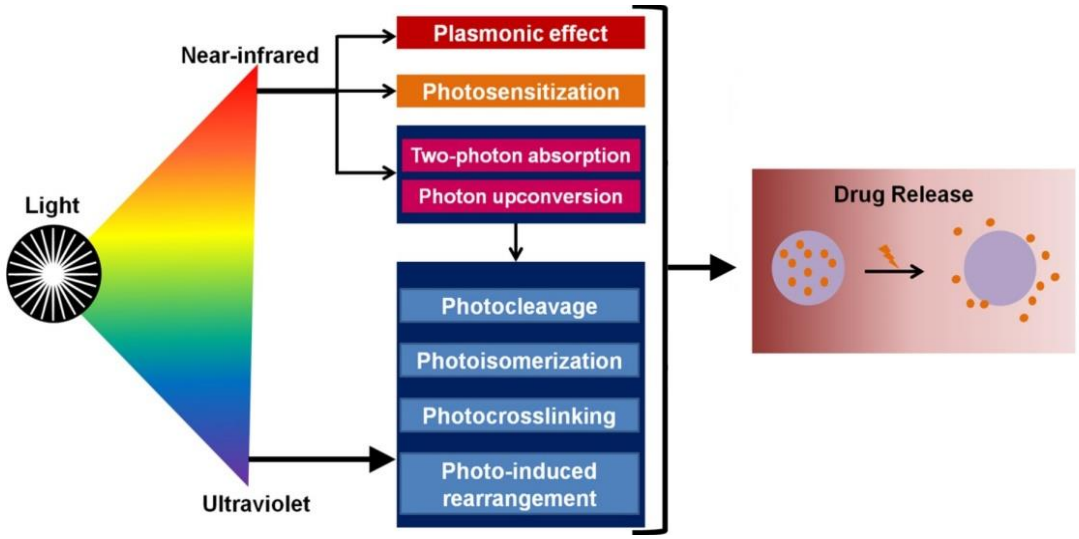

Figure 8. Photo-reaction processes on drug release. Adapted from [52].

Processes based on physical principles

Certain physical phenomena can occur by the application of light on nanomaterials with specific optical properties. For a triggered drug release, most used physical processes include: plasmonic effect [3, 32, 41, 56], upconversion [50, 57] and two-photon absorption [58, 59].

Photo-chemical processes

Photo-chemical processes involve chemical changes at the molecular level which affect nanoparticles properties. Those photo-triggered processes can lead to destabilization or disintegration of the nanoparticles. For nanoparticles disintegration cases, it is often associated the cleavage of covalent bounds. Photo-chemical mechanisms, including photo-crosslinking, photo-isomerization and photo-cleavage, are been extensively used to trigger drug release [60]. In the next section, photo-isomerization and specially photo-cleavage will be described in more detail. Most photo-cleavage processes rely in the use of UV radiation, since it has enough energy to efficiently cleave certain covalent bonds.

3.1. Photo-isomerization

Photo-isomerization is a reversible process in which, upon photo-excitation by a specific wavelength, a photochromic moiety suffers structural changes on a double bond, switching between its isomers, e.g. *E* and *Z* forms [60] (i.e., azobenzene-derivative molecules, see Figure 9) [61].

3.1.1. Azobenzene-derivative photochromic groups

Azobenzene-derivative moieties are one of the most used moieties described in the literature for the development of photo-activatable nanoparticles. Chemically, a *trans* to *cis* isomerization of the azobenzene group, on the rotation-restricted N=N bond, occurs when a UV irradiation (350 nm) is applied. This isomerization can be reverted upon visible light irradiation (450 nm), or by heat [62].

The isomerization is usually incomplete in a way that, in a *trans* to *cis* isomerization it is formed around 80% of *cis*-form in most of the cases and, while *cis* isomer sometimes has a short half life. Additionally, *cis* to *trans* isomerization yields in a 90-95% or higher [63].

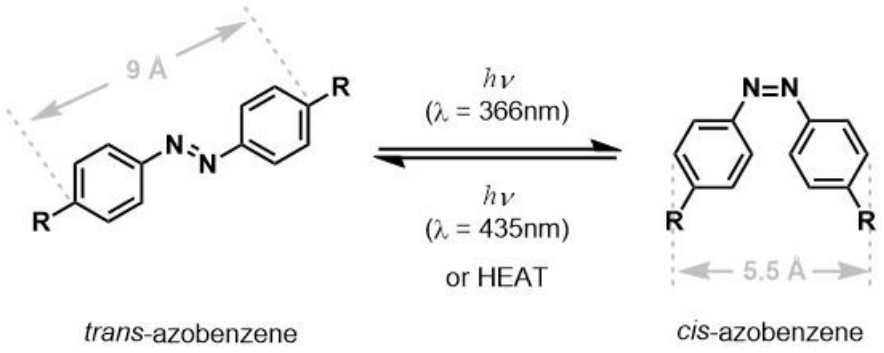

Figure 9. Mechanism of photo-isomerization of azobenzene. Adapted from [62].

Nanoparticles with moieties containing azobenzene groups have been developed for controlled drug release, namely liposomes [64, 65] (Figure 10) and block copolymer NPs [66, 67]. In general, moieties with azobenzene are linked to specific sites of the nanoparticle components and, upon a ≈350nm wavelength irradiation, a switch of *trans*-form to the isomer *cis* leads to changes on the shape, formal size and/or polarity of the nanoparticle and therefore the hydrophilic/hydrophobic balance is altered. As consequence, the nanostructure is destabilized and the drug is released from the nanoparticles.

This leaching process could be reverted by the application of a ≈450 nm wavelength in the system. By irradiating at that wavelength the reversible switch of azobenzene from *cis*-form again to *trans*-form occurs, and thus the nanoparticles recover their stability, stopping the drug release [61].

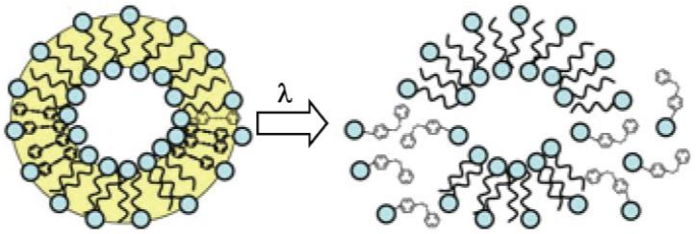

Figure 10. Liposomes containing photo-isomerizable azobenzene moities in trans form: upon light exposure, azobenzene moties trans form changes to its isomeric cis form, leading to liposomes membrane destabilization and consequent drug release. Adapted from [68].

3.2. Photo-cleavage

Opposite to photo-isomerization, photo-cleavage is an irreversible process in which a covalent bond of a photo-labile group is cleaved when irradiated with the proper wavelength. As consequence, two different fragments are generated by the photo-reaction.

3.2.1. *O*-nitrobenzyl-based (*o*-NB) photolabile groups

Among the various photo-labile groups that have been extensively studied until now, *o*-nitrobenzyl-based compounds (*o*-NB) are the most widely used. It's important to highlight, among all the photochemical properties of these compounds, that (1) an *o*-NB alcohol derivative can be photo-cleaved in few minutes (or even seconds) when irradiated with a wavelength in the range 300-365 nm (UV); and (2) the specific wavelength to be applied and the by products that are formed depend on the substituents both at the aromatic ring and linked to the benzylic position [69]. The mMechanism for the photo-cleavage of *o*-NB esters, resulting in *o*-nitrobenzyldehyde formation and the release of a free carboxylic acid, is described in Figure 11.

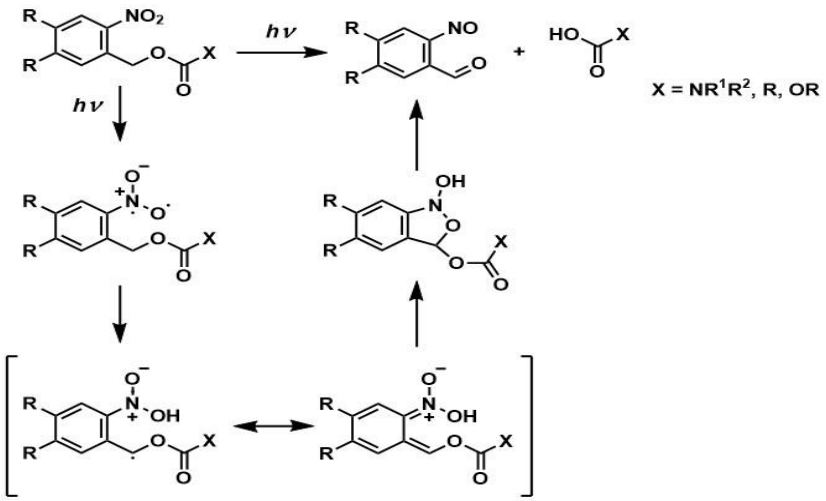

Figure 11. Photochemically-induced cleavage of *o*-nitrobenzyl alcohol. Adapted from [69].

3.2.2. Photo-cleavable nanosystems for drug delivery

o-NB-based moieties have been used in a large number of nanosystems as a strategy for cargo release by light activation, including liposomes and amphiphilic block copolymers (BCP) [51].

In general, there are two main options to introduce photo-cleavable moieties in the nanosystem. One possibility is to use those moieties linked directly to the drug. And so, when linked to the nanocarrier as pendant groups through the "photo-cleavable linker", drug is released by light-triggered cleavage of the connector. The other possibility is to incorporate photo-cleavable moieties in the nanostructure backbone. In this second case, upon light activation of the nanocarrier, photo-cleavable groups are cleaved. This phenomenum leads to the disruption of the nanoparticle and so, drug is released from the nanosystem [31].

Lipid molecules can be modified and used to develop photo-triggerable liposomes. For example, Chandra and coworkers have developed different liposomes obtained from lipids bearing stearylamine non-polar tails (C_{18}-chain fatty acid lipid) linked to charged aminoacids (aspartic acid (Asp), Glutamine (Glu) and Lysine (Lys)) through *o*-NB photo-cleavable moieties. In their work, they show that irradiation of those liposomes at 362 nm, promoting the cleavage of polar groups from the lipids, which results in liposomes disruption and consequent cargo release. They also compared the different liposomes formed by using the set of lipidic molecules. Two main conclusions can be taken from this study: (i) photo-cleavage of liposomes was quicker and more effective in the case of Asp- and Glu-based lipids; and (ii) a controlled release of liposomes cargo occurred in all the cases [70].

Regarding BCP nanoparticles, they are generally constituted by two polymers: one hydrophilic and another hydrophobic. In aqueous medium, the balance between hydrophilic/hydrophobic forces allows the formation of stables micelles, having a corona formed by the hydrophilic subunit of the polymer and a core formed by the hydrophobic subunit. These micelles are able to carry hydrophilic (in the corona) and hydrophobic (in the core) drugs. When the hydrophilic/hydrophobic balance is disturbed, e.g. by the photo-cleavage of the pending chromophores, micelles stability is compromised. This destabilization leads to an increase of permeability or even to the nanoparticle disruption and, as consequence, there is a controlled release of the cargo from the nanosystem (Figure 12) [51].

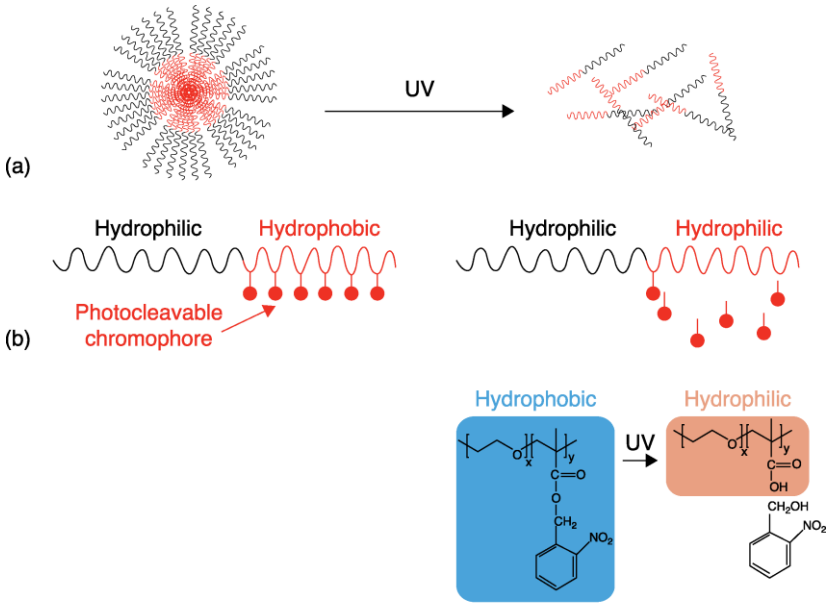

Figure 12. Photo-cleavable polymeric micelles. (a) Scheme for photo-dissociation of a diblock copolymer micelle. Photo-cleavage of chromophores renders hydrophobic block copolymer hydrophilic, leading to micelles dissociation (b) Chemical structure and photoreaction of amphiphilic diblock copolymer containing *o*-nitrobenzene. Adapted from [51].

Expecifically, *o*-nitrobenzyl moieties can be introduced in these BCP-based systems. As mentioned, photo-cleavage causes a change in the hydrophilic/hydrophobic balance and induces micelles disruption. An example are those BCP-nanoparticles developed by Jiang and coworkers, constituted by a hydrophilic block of Poly (ethylene oxide) (PEO) and a hydrophobic block of poly(methacrylate) (PMA) with *o*-nitrobenzyl esters as pendant group (Figure 13) [71]. In this work, autors create a novel and effective approach to design amphiphilic block copolymers able to form photo-cleavable micelles in aqueous solution (by using photo-cleavable chromophores). The ability of their developed BCPs to release efficiently Nile Red dye was also shown. This strategy can be readily applied to many chromophores or dyes, being a great contribute in BCP development for efficient cargo delivery.

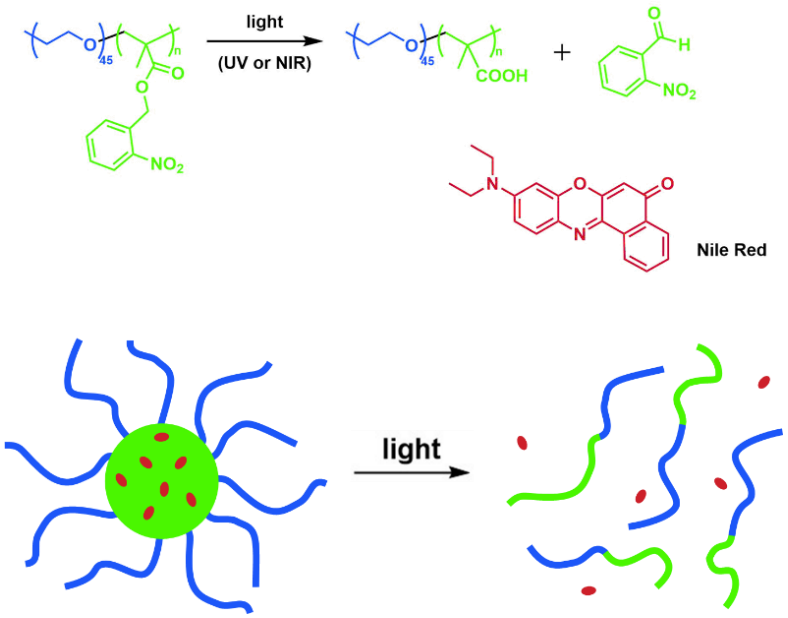

Figure 13. Top: Photolysis of the *o*-nitrobenzyl-containing amphiphilic block copolymer and chemical structure of Nile Red. Bottom: Schematic illustration of the photocontrolled release of encapsulated Nile Red as a result of the photoinduced dissociation of the polymeric micelle. Adapted from [71].

Oposite to burst release, Liu and coworkers have also developed a photo-cleavable BCP which forms micelles that slowly release their cargo after light activation. In their work, they synthesized a poly(S-(*o*-nitrobenzyl)-Lcysteine)-*b*-poly (ethylene glycol) diblock copolymer (PNBC-*b*-PEO). These copolymer forms micelles in water which, after photo-cleavage of *o*-NB groups, shrink leading to a gradual doxorubicin (DOX) release (Figure 14) [72].

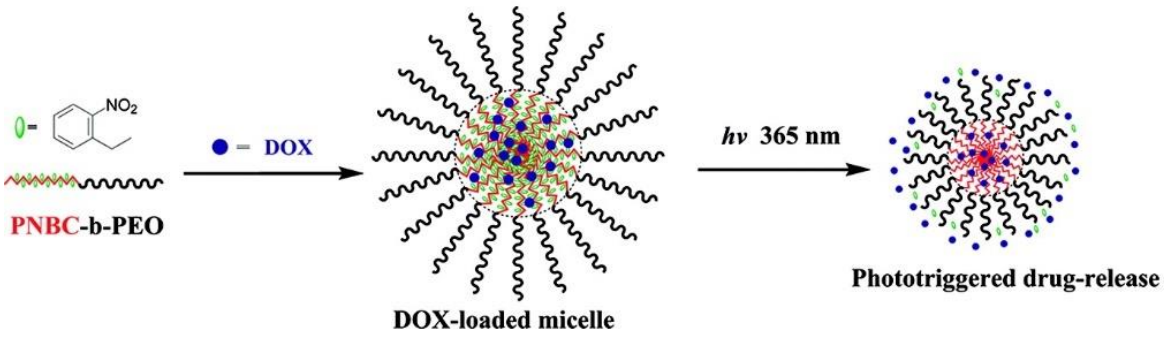

Figure 14. Illustration of self-assembly and photo-triggered drug-release from photo-responsive PNBC-*b*-PEO copolymer block in aqueous solution. Adapted from [72].

4. Intracellular siRNA delivery by nanoparticles

4.1. General insights

In order to develop an efficient system for siRNA delivery, it is important to understand the mechanism by which these carriers are internalized. Several studies have been done in order to understand the mechanism of lipidic and polymeric nanoparticles internalization and trafficking [73, 74]. As a result of these studies, a general model is proposed (Figure 15). Regarding this model, after introduced into the body, the cellular uptake of nanoparticles occurs mainly by endocytosis pathways and are included in vesicles called endosomes. Inside the cell, endosomes suffer a maturation process until they reach a late endosome state and form lysosomes. Gilleron and coworkers showed (for the first time) that lipoplexes (lipid nanoparticles complexed with siRNA) escape from early endosome and are delivered to the cytosol, escaping to degradation and exocytosis. However, only **less than 2% of the total amount is able to escape** from endosomes. The rest of these nanoparticles with siRNA suffers an endosomal recycling process or they are even expelled by exocytosis [75].

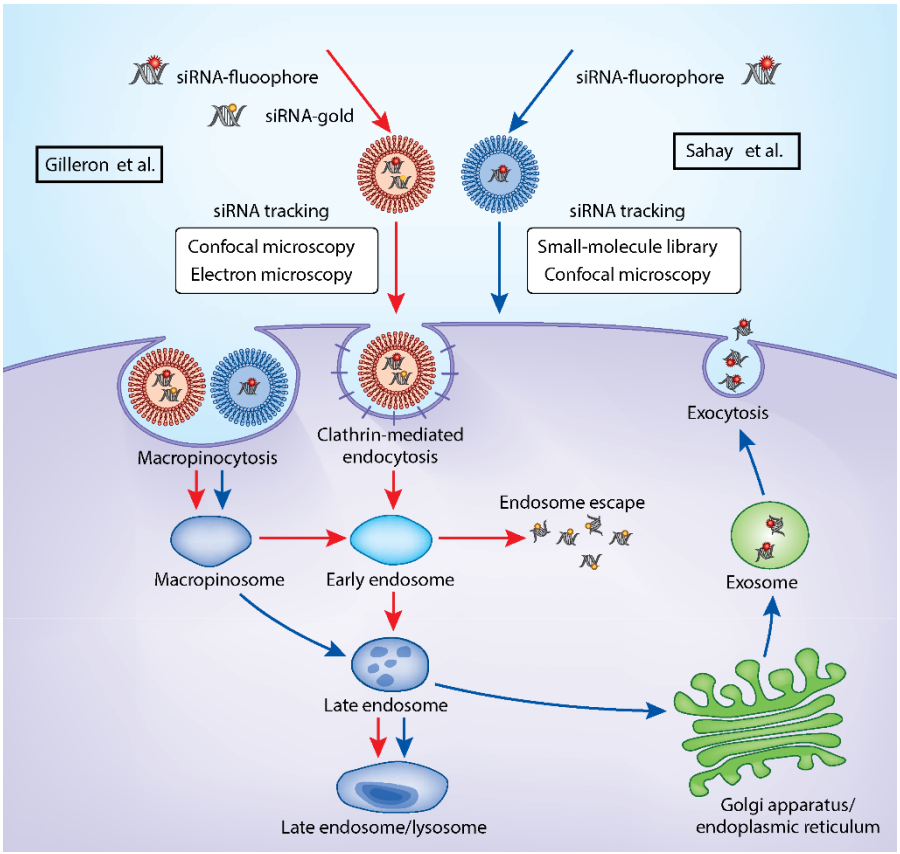

Figure 15. Schematic model of the intracellular uptake and trafficking of siRNA carried by lipid-based nanocarriers. Adapted from [76].

For an efficient and safe siRNA delivery into the cells, several barriers should be overcomed (Figure 16) [77, 78]:

- **siRNA stability**: siRNA is prone to degradation by pH changes or enzymes, which is a big issue for its 'naked' delivery. On the other hand, since siRNA are hydrophilic and negatively charged molecules, they tend to aggregate with serum proteins, which is harmful for biological systems.
- **Targeting**: circulation time of free siRNA in the bloodstream is low. The hydrophilicity of siRNA is an issue since it leads to its rapid clearance. Additionally its negative charge can difficult the interaction between siRNA and targeted cells, since cell membranes are negatively charged.
- **Endosome escape**: Several macromolecules are uptaken by endocytosis and carried to lysosomes. In lysosomes, pH conditions and enzymes compromise siRNA stability, so siRNA must be able to escape from early endosomes in order to reach the cytosol, which is also an issue for free siRNA.

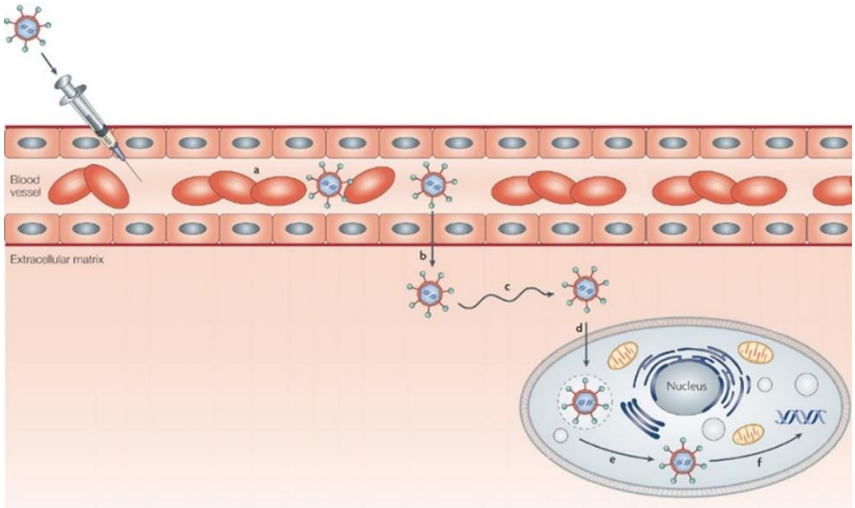

Figure 16. Physiological barriers for the systemic delivery of siRNA. After injection, nanoparticles must be able to: avoid phagocytosis and degradation in bloodstream (a); cross blood vessels (b); diffuse through the extracellular matrix (c); be uptaken and internalized in the cell (d), escape from endosome (e) and release efficiently siRNA to the iRNA machinery. Adapted from [79].

4.2. Nanoparticles for siRNA delivery

To overcome the challenges related with siRNA delivery, several nanoparticles have been developed in order to protect, improve targeting and facilitate uptake, internalization and siRNA trafficking. Positively-charged nanoparticles (cationic) have high potential for the efficient intracellular delivery of siRNA. Besides all the general advantages of nanoparticles, cationic nanoparticles have two key advantages broadly described in the literature [80]: (i) they have a positive net charge and thus are more effective in the complexation of siRNA and potentially in the interaction with negative charge cell membrane, and (ii) they are likely

to be more effective in escaping the endolysosomal compartment (Figure 17). In general, this last phenomenon consists in the activation of proton pumps by cationic nanoparticles with pH-buffering properties. As a result, osmotic pressure inside endosome increase and thus endosome swelling and bursting with subsequent carrier escape from it. Additionally, it is also described that some cationic lipids interact with anionic lipids from the endosome, causing endosomes membrane destabilization and thereby leading to endosome escape of NP-siRNA complexes.

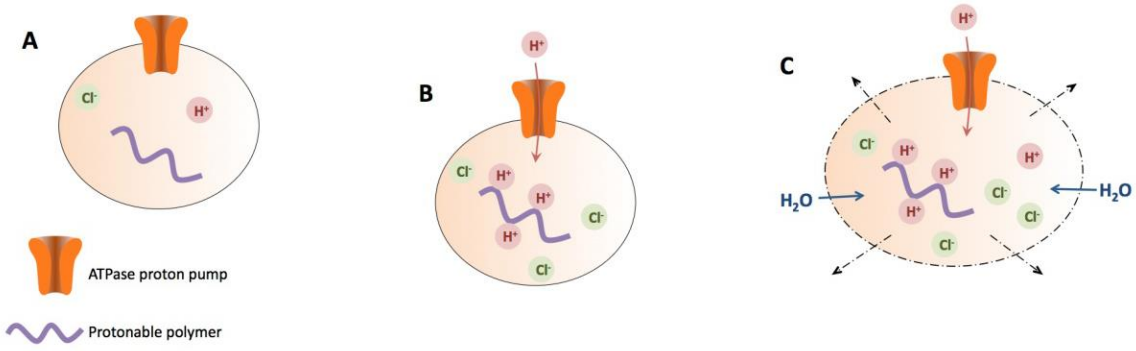

Figure 17. Schematic representation of the *proton sponge effect*. Adapted from [80].

There are two major classes of cationic nanoparticles used for the release of siRNA: lipoplexes and cationic polymeric nanoparticles. Lipoplexes are cationic lipidic nanoparticles complexed with siRNA [81]. A large number of cationic lipids for siRNA delivery have been developed [82] and the transfection efficiency of these vectors depend on: chemical structure of lipoplexes, ratio between the lipid charges , charge ratio cationic-lipid/siRNA, size and structure. Lipofectamine 2000 is a cationic lipid successfully implemented in the market which, due to its high transfection efficiency is currently widely used for siRNA delivery [83]. However, its application still is limited, due to its high cytotoxic effect [84]. From the currently developed lipoplexes for siRNA delivery, the most promising have in their constitution "helper" neutral lipids, such as 1,2-dioleoyl-*sn*-glycero-3-phosphoetanolaine (DOPE) or poly(ethyleneglycol) (PEG) conjugated with neutral lipids. DOPE is involved in endosomal escape after endocytosis of lipoplexes and PEG-conjugated neutral lipids increase *in vivo* lipoplexes stability.

Cationic polymers may complex siRNA forming polyplexes. Polyplexes, such those obtained from poly(ethyleneimine) (PEI), poly(lysine), poly (ß-amine esters), poly(amidoamine) (PAMAM) and poly(propylamine) dendrimers have been widely used as carriers for *in vivo* and *in vitro* gene delivery [85]. Due to its high capacity to escape from endosomes, PEI is a good example of a polymeric transfection agent. It is an agent with powerful transfection capacity however presenting some cytotoxicity issues [86]. Poly (ß-amine esters) nanoparticles have been shown to have a high potential for efficient siRNA delivery with similar efficiency as PEI [87, 88].

- This page was intentionally left blank

Chapter 3: Materials and Methods

1. Materials

The poly (amino amide)-based polymer used for nanoparticles synthesis was previously prepared in the lab and kindly provided by Josephine Blersch. Molecular grade RNAse-free sterile water used throughout the experiments was supplied by 5PRIME GmbH. Zinc sulfate heptahydrate ($ZnSO_4.7H_2O$) and potassium chloride (KCl) were purchased from Sigma Aldrich. siRNA GFP duplex I (stock concentration 266 µg/mL) and CY5 modified siRNA GFP Duplex I (stock concentration 298 µg/mL) were purchased from Invitrogen.

For cell culture, fetal bovine serum (FBS, 72442) was purchased from Sigma Aldrich. Penicillin and Streptomycin (pen/strep) (each antibiotic in concentration 10.000 U/mL), were acquired from Lonza. For Hela and HeLa-GFP cell culture, four culture media were used: i) Dulbecco's Modified Eagle Medium (DMEM, Gibco) supplemented with L-glutamine (stock concentration 200 mM, Gibco), pen/strep solution and 10% FBS, for normal cell growth; ii) Dulbecco's Modified Eagle Medium (DMEM, Gibco) supplemented with L-Glutamine (stock concentration 200 mM, Gibco), pen/strep solution and 5% FBS, for controlled cell growth; iii) DMEM with L-Glutamine and phenol red (Biochrom, Merck) supplemented with pen/strep solution and 10% FBS; and iv) DMEM with L-Glutamine and phenol red (Biochrom, Merck) supplemented with pen/strep solution and 5% FBS.

For Hela-GFP culture, antibiotic A1113903 Blasticidin S HCl with a stock concentration of 10 mg/mL, was purchased from Gibco. Dulbecco's Phosphate Buffered Saline (PBS) for cell washing was purchased from Biochrom, Merck. Trypsin-EDTA solution (0.5%) was supplied by Gibco. Trypan blue (0.4%) was supplied by Lonza and solutions of propidium iodide (PI) and Hoechst 33342 (H33342) stains were purchased from Sigma.

2. Equipments

For nanoparticles lyophilization we have used a freeze-dryer (Snijders Scientific). For nanoparticles photo-activation, a UV lamp (UVP®), Transilluminator (UVP®) and a manual laser (blue light, 405 nm) were used as light sources. DLS analyses were performed in a Brookhaven Instruments Corporation's equipment and imaging analysis was done in a InCell analyser 2200 equipment (GE Healthcare Life Sciences). A Spectrophotometer/Fluorometer (BioTek HT) was used for UV/Vis assays and fluorescence measurement.

3. Synthesis of nanoparticles

Nanoparticles were prepared by precipitation of the poly(aminoamide)-based polymer C11- linked to photo-cleavable pendant DMNC moieties (15 µl) in molecular grade nuclease free water (960 µl), containing 1M $ZnSO_4 \cdot 7H_2O$ (25 µl). The resulting suspension was then

shaked overnight (25ºC, 250 rpm). Two types of nanoparticles were prepared based in the (1) non-purified C11 and (2) purified polymer C11_P. After preparation, the nanoparticles were purified by centrifugation (4ºC, 8000 g, 8 min), aliquoted, frozen in liquid nitrogen and stored at -80ºC until use.

To determine the NP stock concentration, 2 mL of each NP formulation were used and purified by centrifugation. After removing the supernatant, NPs were freeze dried overnight and the mass of the NP pellet was determined. Mass concentration of NPs was calculated as in Equation 1.

$$\frac{(mass\ after\ freeze{-}drying\ -\ mass\ before\ freeze{-}drying)}{2} = \boldsymbol{X}\ \mathrm{mg/mL} \qquad \text{Equation 1}$$

4. Complexation of nanoparticles with siRNA

Nanoparticles were complexed with siRNA at a 50:1 ratio. siRNA stock solution (8 µg/mL) was prepared, using a 1:1 ratio of non-labelled siRNA GFP Duplex I and CY5-labelled siRNA GFP Duplex I, diluted in a molecular grade nuclease free sterile water. For the complexation, a volume of siRNA stock solution was taken and added to a volume of NP suspension, to have a final concentration of 200 µg/mL of NP. The complexation was performed in an orbital shaker for 2h (25ºC, 250 rpm).

To determine complexation efficiency, samples were diluted in DMEM (10 times) to a final concentration of 20 µg/mL of NP@siRNA complex. Samples were then centrifuged (4ºC, 1400 G, 15 minutes), supernatants were collected and CY5 fluorescence of CY5-tagged siRNA was analysed for each sample by fluorescence spectrophotometry. The values obtained were compared to a standard curve of CY5 fluorescence (**Erro! A origem da referência não foi encontrada.**).

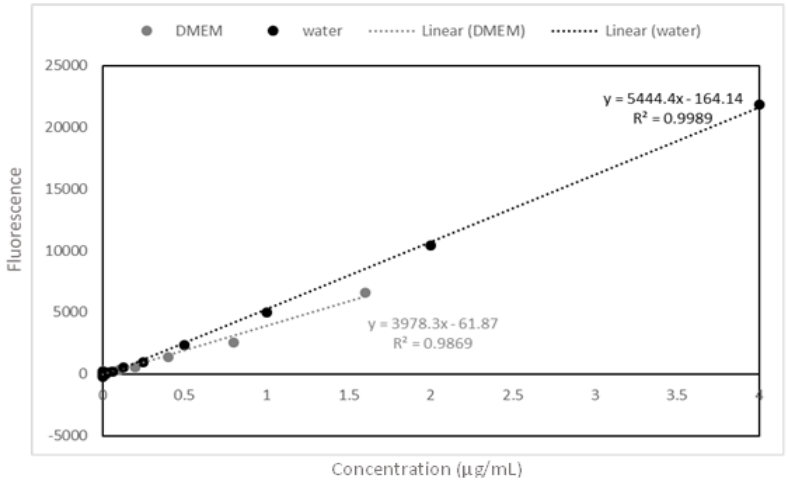

Figure 18. Calibration curve for calculation of NP@siRNA complexation efficiency. Complexation of nanoparticles with siRNA (20 µg/ml NP) during 2h in orbital shaker. In the spectrophotometer, it was used a filter set 1; λ_{ex} = 649 nm, λ_{em} 675 nm; light source: xenon flash, lamp energy high; Measurements/data points: 10.

5. Nanoparticle characterization

5.1. Dynamic light scattering (DLS) and phase analysis light scattering (PALS)

DLS, also known as Quasi-elastic Light Scattering (QELS) or photon correlation spectroscopy, is the common method to determine the size distribution (diameter, nm) of nanoparticles in suspension. It is a non-destructive method. DLS is based on the constant random motions (Brownian motions) of particles in solution or suspension and relate their speed with particles size. Because these motions are random, when applied a light beam, light is scattered in all directions, depending on particles diffusion. Intensity fluctuations of light scattered in a specific angle are analysed and, by this way, speed and subsequently the size of the particles can be determined overtime (Figure 19). Since DLS determines particle size by the hydrodynamic radius of a virtual sphere, this method adjusts size distribution to spherical particles.

C11 (stock concentration 2.28 mg/mL) and C11_P nanoparticles (stock concentration 1.0 mg/mL) were characterized in terms of size using a 90PLUS Particle Size Analyzer equipment (Brookhaven Instruments corporation). Previously, it was observed that the DLS equipment give more significant results when suspension have Kcps (kilo-counts per second) in a range between 100-200 Kcps. In order to achieve this range, samples were diluted before measurements. Dilution was done in KCl 1 mM, pH 5.5, a standard solution for DLS and zeta potential measurements.

After measurement of the size of nanoparticles, size of nanoparticles complexed to siRNA was determined before and after photo-activation with UV and blue laser (power intensity: 100 mW/cm^2; time irradiation: 10 minutes).

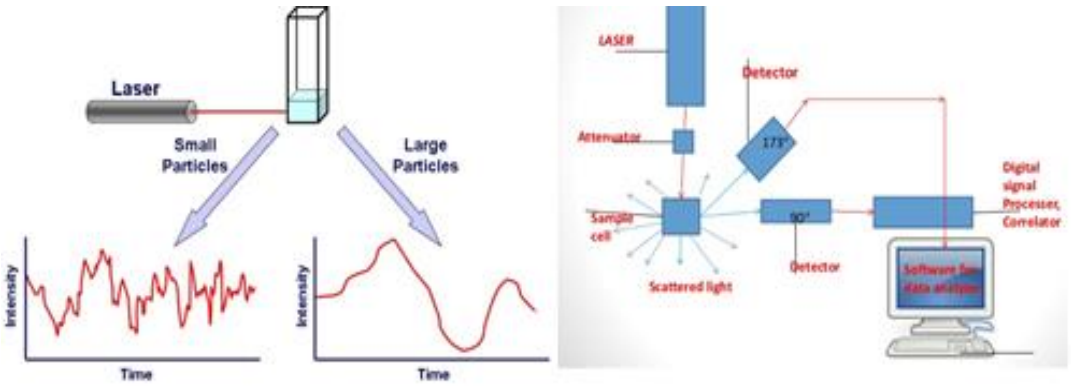

Figure 19. Dynamic Light Scattering (DLS). a) Fluctuations of light intensity and Brownian motions. Small particles migrate faster and so fluctuations of light scattered are more intense comparing with large particles. b) Scheme of a DLS equipment, adapted from http://www.azom.com/article.aspx?ArticleID=12255 and http://www.slideshare.net/poojabhartii3/dynamic-light-scattering, accessed on 12th June 2016.

Zeta potential is a parameter defined by the charge of a particle together with all the molecules (e.g. ions) adsorbed to its surface (Figure 20). The zeta potential can be measured by PALS (Figure 20). In this method, an electric field is applied to the suspension, forcing the movement of the particles to each electrode according to their charge. The migration of the particles depends on the applied field and the zeta potential associated to the particles. The applied field is known and so is easy to know also the zeta potential value.

Zeta potential of C11and C11_P nanoparticles and NP@siRNA complexes was determined via ZetaPALS Analyzer software (Brookhaven Instruments corporation) before and after light activation (power intensity: 100 mW/cm^2; time irradiation: 10 minutes). Data was recorded at 90º angle, temperature of solution 25ºC, in 5 runs. Samples were diluted before measurements in KCl 1 mM, pH 5.5, achieving 100-200 Kcps.

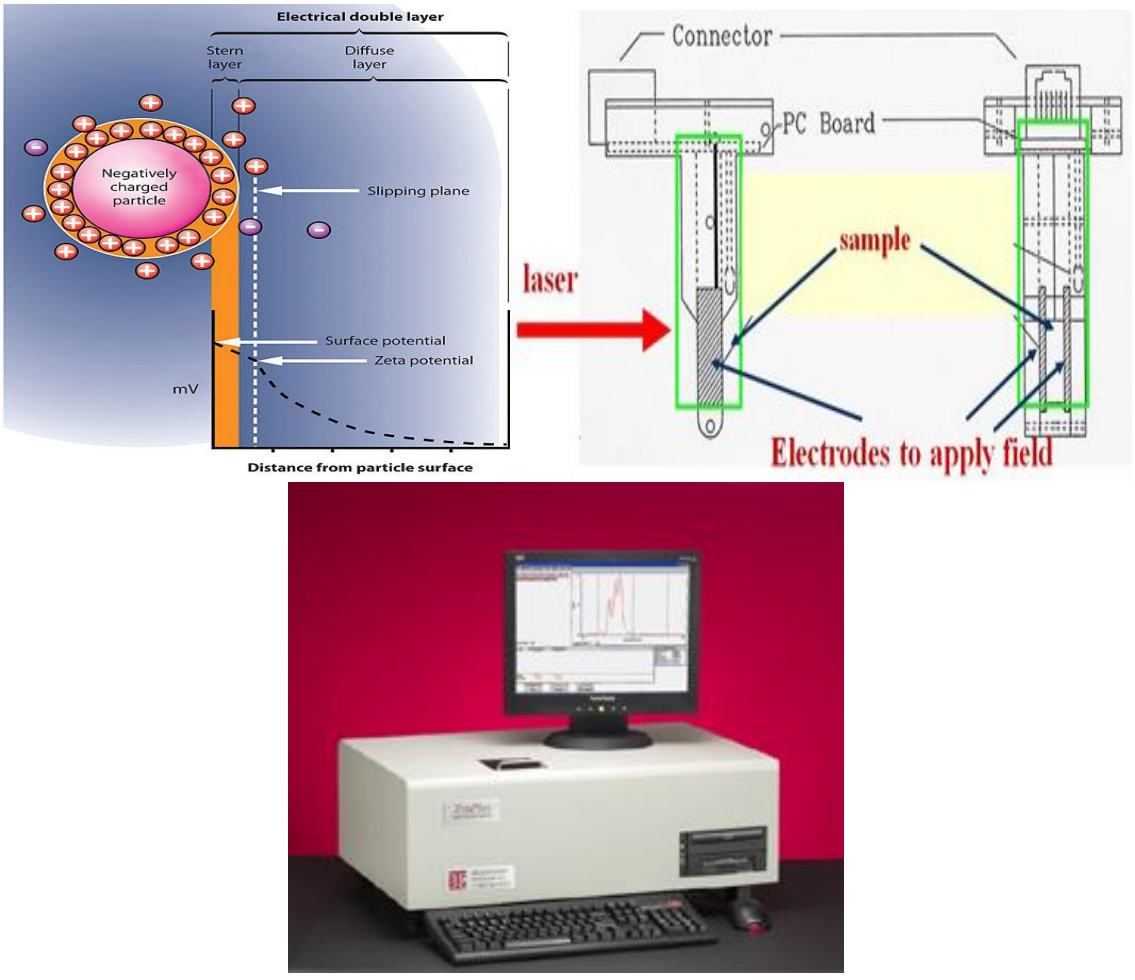

Figure 20. Zeta Potential measurements. A) Scheme illustrating zeta potential. b) Particle Size Analyzer (90PLUS) and Zeta Potential Analyzer (ZetaPLUS), adapted from http://www.pcimag.com/articles/91076-paint-formulations-and-the-need-for-zeta-potential?v=preview, accessed on 12th June 2016.

5.2. Light-trigger nanoparticles disassembling

To assess if nanoparticles respond to UV/blue laser, kilo count per second (Kcps) values were analysed from the size measurement in the Brookhaven ZetaPALS. Kcps can be related with the concentration of nanoparticles in suspension. Knowing Kcps before and after light activation, we can calculate the % of count decrease (Equation 1), that can be related with the decrease of nanoparticles in suspension. With the decrease of nanoparticles in suspension, it is possible to infer about nanoparticles disassembly and so its photo-responsiveness.

$$\frac{(Kcps\ before\ light\ activation - Kcps\ after\ light\ activation)}{Kcps\ before\ light\ activation} = X\ \% \qquad \text{Equation 1}$$

The photo-dissassembly of the nanoparticles was also confirmed by spectrophotometry. Spectrophotometry is a quantitative method to determine the concentration of a substance in a solution which absorbs radiation at a specific wavelength. In general, a beam light passes through the sample and the amount of light that reaches the detector is measured. This amount of light detected, depends on the light absorbed by the sample. Using Lambert- Beer Law, it is possible to calculate the concentration of a molecule in solution knowing the absorbance of the same molecule, since, in the range of values where the Lambert- Beer Law is applicable, concentration and absorbance of a molecule are directly proportional.

In order to confirm if UV (365 nm) and blue laser light (405 nm) conditions tested were enough to disassemble the photo-activatable nanoparticles. C11 and C11_P nanoparticles solution (200 µg/mL) were photo-activated with UV and a blue laser light (power intensity: 100 mW/cm^2; time irradiation: 10 minutes). Then, the absorbance of total nanoparticles solution, as well as supernatant and the resuspended nanoparticle pellet (200 µg/mL) after centrifugation ((4ºC, 8000 g, 8 min) were measured in a UV/vis spectrophotometer. The spectra were obtained in the range of 270-600 nm with 4 nm stepwidth.

6. Cell culture

In vitro studies were performed using a stable HeLa-GFP reporter cell line, purchased from Cell Biolabs, Inc. For *in vitro* assays, HeLa cells and HeLa cells expressing GFP were cultured in tissue culture flasks (T75) using DMEM supplemented with 10% FBS, 0.5% pen/strep solution, pH 5.5. For HeLa-GFP selection, medium was also supplemented with 0.1% blasticidin, pH 7.5 at 37ºC, 5% CO_2.

Cell harvesting (T75 flasks) was initiated by washing the cells with PBS Dulbecco's solution (5 mL) followed by cell incubation with 0.5% trypsin-EDTA solution (2 mL) for 3 minutes. Trypsin was inhbited with DMEM containing 10% FBS, 0.5% pen/strep solution (5 mL). After centrifugation (300 rpm, 3 minutes), cells were resuspended in 2 mL of DMEM with 10% FBS,

0.5% pen/strep solution and 0.1% blasticidin in case of HeLa-GFP cells. Cells were counted in a Neubauer Chamber (see supplementary material). Live cells were differentiated from dead cells using a trypan blue solution (0.4%). Cells were further seeded in 96well plates in a concentration of 4.000 cells/well using DMEM supplemented with 10% FBS, 4 mM L-Glutamine (stock concentration 200 mM) and incubated overnight at 37ºC, 5% CO_2 before experiments.

7. Cell transfection

Cells were transfected with C11@siRNA and C11_P@siRNA complexes after previous 10 times dilution, in order to achieve 20 µg/mL of nanoparticles. For transfection, the culture medium in which cells were cultured was removed. Then, siRNA-NP complexes (20 µg/mL of nanoparticles) were used to transfect cells (10 minutes' incubation). After transfection time, transfection cell cocktail was removed and replaced by 100 µl/well of DMEM supplemented with 5% FBS, 4 mM L-Glutamine, 0.5% of Pen/strep solution and 0.1% of blasticidin in case of HeLa-GFP cells, pH 7.5. Transfected cells were photo-activated (UV: 365nm, power intensity: 1 mW/cm^2; time irradiation: 10 minutes; blue laser: 405 nm, power intensity: 10 and 20 mW/cm^2; time irradiation: 30 second, 1 minute and 3 minutes) and incubated at 37ºC, 5% CO_2 until staining.

8. Cell staining and imaging

Cells were stained with a solution containing propidium iodide and Hoechst H33342 (0.25 µg/mL) for 15 min. Cells were analysed on an automated fluorescence microscope (InCell 2200 Analyzer) 48 h post transfection. 4 images per well were analysed.

Automated image analysis was performed by the InCell developer software (Figure 21), using specific protocols previously established in the lab (by Josephine Blersch). Based on the nucleus staining with H33342 a nucleus mask was defined. Dead nuclei could be identified by PI staining. If there was an overlap of 10% between nucleus mask and PI staining, nuclei were defined as dead nuclei. Using Equation 2, the cell viability was calculated.

$$100 - \frac{(dead\ nucleus * 100)}{total\ nucleus} = X\ \% \qquad \text{Equation 2}$$

Next, the GFP knockdown was determined by GFP fluorescence intensity measured in the cytoplasm of healthy cells. This analysis was perfomed creating an artificial cytoplasm on the base of the nucleus staining (Figure 21), since GFP signal was expected to deplete in the process of knockdown. A healthy cell population was achieved, by subtracting PI positive nuclei from the nucleus and also excluding nuclei with a form factor >0.95. Nuclei were then dilated to cells. Slightly dilated nuclei (to avoid signal contamination of H33342 in GFP) were then subtracted from artificial cell mask to achieve the cytoplasm. Mean GFP fluorescence intensity was measured in that mask and GFP knockdown was calculated as in Equation 3.

$$100 - \frac{((cytoplasm\ cells\ fluorescence - mean\ HeLa\ control\ fluorescence) * 100)}{mean\ HeLa - GFP\ control\ fluorescence} = X\ \%$$ Equation 3

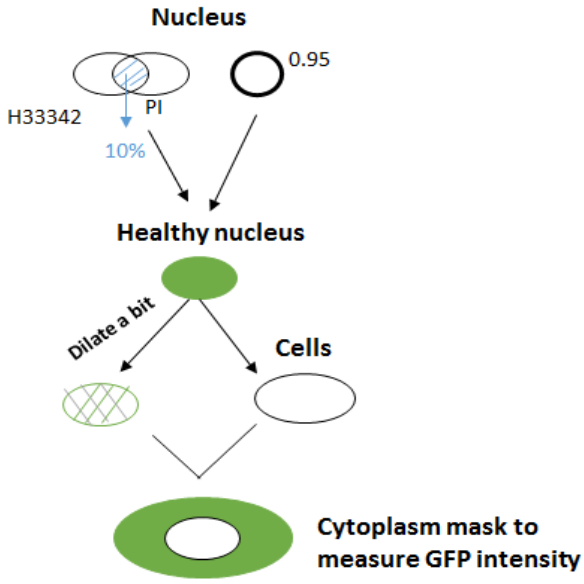

Figure 21. Scheme illustrating analysis InCell developer. Healthy nucleus is masked with H33342 staining and dead cells masked with PI staining. Healthy nucleus population is defined by subtraction of the overlap area (≥10%) between PI and H33342 masked nucleus. Rounded cells with a factor > 0.95 are also considered dead and subtracted when healthy nuclei population is defined. Since H33342 staining contributes to GFP fluorescence increase, in order to decrease this artefact in GFP signal, the nucleus maskis dilated a bit. Then, an artificial cytoplasm is created in the cell by expansion of healthy nuclei to cells and subtraction oh the nucleus from cells. Then, Mean GFP fluorescence intensity (green) in the cytoplasm is measured.

9. Images and statistical analyses

Each experiment, was performed using three technical replicates (n=3) in a 96 well plate and final results were presented in Mean values±SEM. Analysing the success of the experiment by fluorescence microscopy with InCell 2200, four fields were imaged per replicate, obtaining a representative data from the whole well. Automated image analysis was performed for those images by using the InCell developer Software. Statistical analyses were performed by Graphpad® software. Results are presented as Mean value ± standard deviation from three technical replicates. Two-tailed student's T-test and one-way analysis of variance (ANOVA) were performed to compare two or multiple groups of independent samples (each condition was compared to control conditions), respectively. Differences were once considered significant at $P \leq 0.05$.

– This page was intentionally left blank –

Chapter 4: Results and Discussion

1. Nanoparticles characterization

Two nanoparticle formulations were initially produced from C11 polymer either purified (C11_P) or non-purified (C11). The size and zeta potential of the nanoparticles, before and after complexation with siRNA, were determined using DLS and PALS respectively (see Chapter 3). Nanoparticles were resuspended in a standard KCl solution. Results are presented below in Figure 22 and Figure 23. C11-NPs and C11_P-NPs have a size of 118±0.2 nm (Mean diameter) and 61±0.064 nm, respectively. Both formulations present a positive zeta potential: 22.7±1.15 mV for C11-NP and 15.15±1.27 mV for C11_P-NP. This positive zeta potential is likely explained by the presence of amine groups in the nanoparticles.

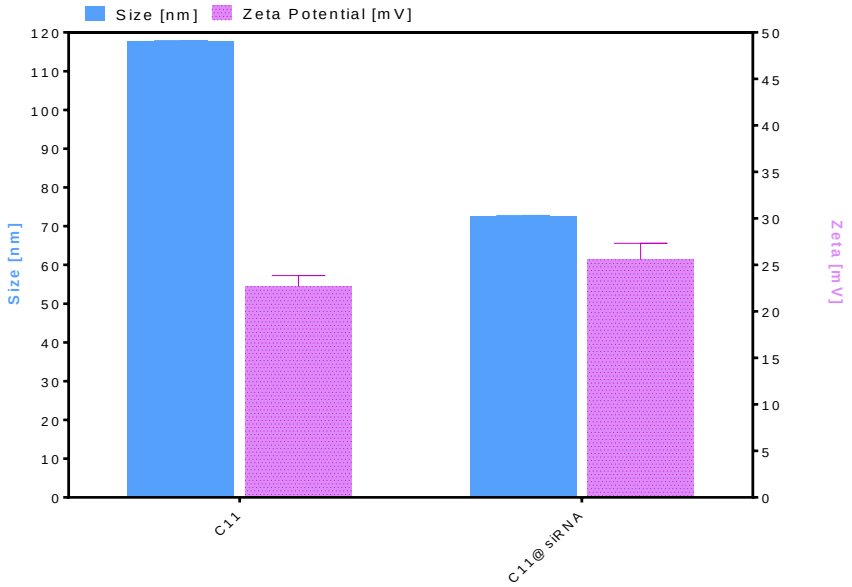

Figure 22. Characterization of C11 nanoparticles. The size and zeta potential of C11 and C11@siRNA nanoparticles (2 mL, 28.5 µg/mL in KCl 1 mM solution) were evaluated by dynamic light scattering (DLS) and phase analysis light scattering (PALS), respectively. Before measurements, samples were allowed to equilibrate 5 minutes, in order to stabilize the dispersion. Size was given by diameter of hydrodynamic radius and zeta potential was obtained during 5 runs, measuring 3 values in each run. Results are expressed as Mean ± SEM (n=3).

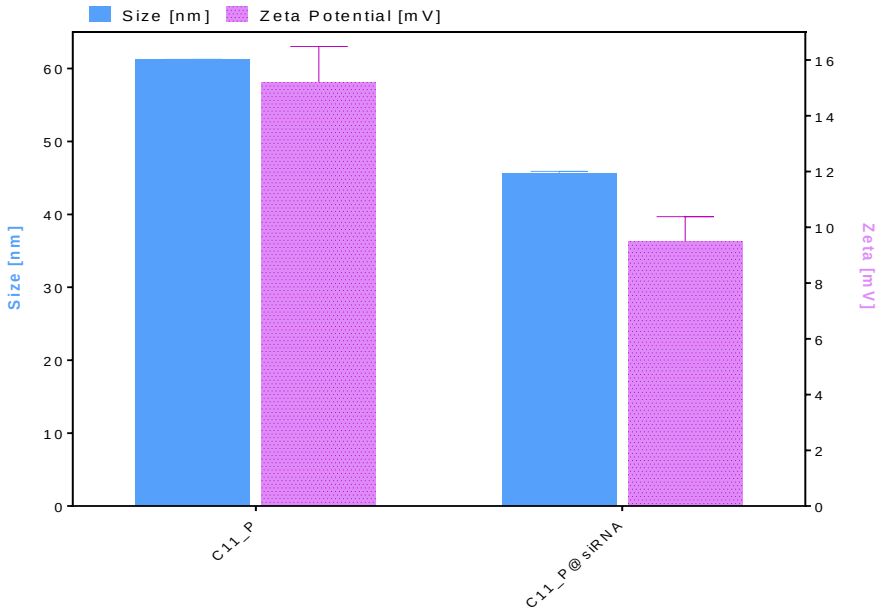

Figure 23. Characterization of C11_P nanoparticles. The size and zeta potential of C11_P and C11_P@siRNA nanoparticles (2 mL, 28.5 µg/mL in KCl 1 mM solution) were evaluated by dynamic light scattering (DLS) and phase analysis light scattering (PALS), respectively. Before measurements, samples were allowed to equilibrate 5 minutes, in order to stabilize the dispersion. Size was given by diameter of hydrodynamic radius and zeta potential was obtained during 5 runs, measuring 3 values in each run. Results were expressed as Mean ± SEM (n=3).

After complexation with siRNA (GFP Duplex I and CY5-labelled siRNA), nanoparticles present a smaller size relatively to the nanoparticle formulations. Interestingly, C11 and C11_P nanoparticles show similar positive zeta potential values. It was anticipated a decrease in zeta potential values after nanoparticles complexation with siRNA, due to the negative charge of siRNA. Therefore, this indicates that C11 nanoparticles have a high capacity to compensate siRNA negative charge. In contrast, this is not occurring for C11_P nanoparticles after siRNA complexation, and so these nanoparticles resulting from the purified polymer seem to lose the capacity to compensate negative charge.

2. Light-disassembling of nanoparticles

Next, the light-disassembling process of nanoparticles was studied by DLS. Nanoparticles suspended in water were exposed to UV (365 nm) or blue laser (405 nm) during 10 minutes, at 100 mW/cm^2 in both cases (Table 1). Our results show that C11@siRNA and C11_P@siRNA nanoparticle size increased after light activation. It is possible that the cleavage of hydrophilic DMNC moieties from the polymer increased nanoparticles hydrophilicity and thus their swelling. Most probably, decrease in size can only be observed after certain time (minutes, even hours depending on the polymer). However, it wasn't measured during this work. However, the number of nanoparticles, as evaluated by nanoparticles in suspension per second (Kcps), decreased after light irradiation. C11_P-NPs are much less photo-responsive

when blue laser is applyied (around 37-38% count decrease) than nanoparticles resulting from the non-purified polymer C11 (between ~89% count decrease). It is likely that the loss of short molecular weight polymers removed by dialysis (purification process) affected the nanoparticle disassembling process. By forming nanoparticle from purified polymer C11_P, only the longer polymeric chains will be part of the coacervate, and so, stability of the resulting nanoparticle is much higher and less depending in hydrophobic/hydrophilic interactions.

Table 1. Physicochemical properties of C11@siRNA and C11_P@siRNA nanoparticles after light activation (UV, 365 nm and blue laser, 405nm; power at 100 mW/cm^2 during 10 minutes). Results are expressed as Mean ± SEM (n=3).

Nanoparticles	Light activation	Size [nm]	Zeta Potential [mV]
C11	Non-irradiated	117.7±0.20	22.7±1.15
C11@siRNA	Non-irradiated	72.5 ± 0.27	25.59 ± 1.74
	365 nm	156.6 ± 0.08	21.79 ± 1.53
	405nm	219.4 ± 0.12	20.64 ± 1.99
C11_P	Non-irradiated	61.2 ± 0.06	15.21 ± 1.27
C11_P@siRNA	Non-irradiated	45.7 ± 0.20	9.5 ± 0.88
	365 nm	76.3 ± 0.16	6.51 ± 0.44
	405 nm	75.7 ± 0.10	7.06 ± 1.72

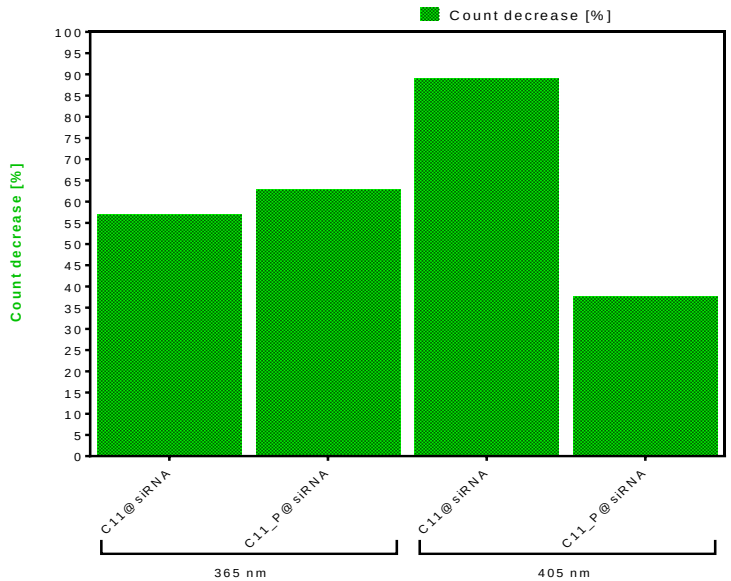

Figure 24. Effect of the light in nanoparticles disassembly. C11@siRNA and C11_P@siRNA complexes (2 mL, 28.5 µg/mL in KCl 1 mM solution) were exposed to UV light (365 nm, 100 mW/cm^2) and blue laser (405 nm, 100 mW/cm^2), during 10 minutes. Kcps values before and after light activation were determined. Results are expressed as Mean ± SEM (n=3).

In order to assess if the quantum yield of UV and blue laser light conditions are enough to trigger nanoparticles disintegration, UV/vis spectrophotometry measurements before and after light activation were performed for both C11 and C11_P nanoparticles. Absorbance spectra were recorded after centrifugation for both, supernatant and resuspended nanoparticles, before and after light activation (365 nm and 405 nm, 100 mW/cm^2, 10 minutes) and were compared in a range between 270 and 600 nm. Results are presented below.

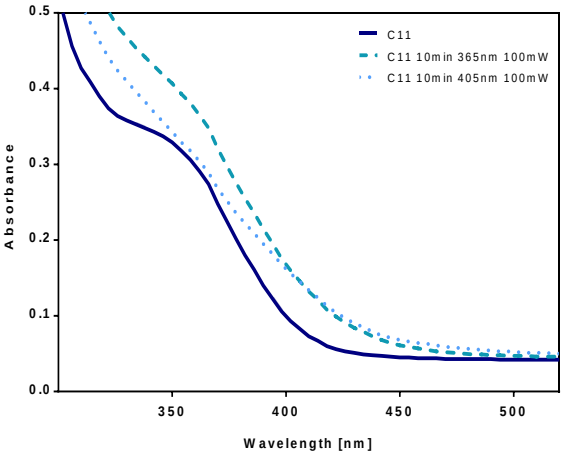

Figure 25. UV/vis spectrum of C11 nanoparticles (200 µg/mL) supernatant before and after UV (365 nm, 10 minutes, 100 mW/cm^2) and blue laser (405 nm, 10 minutes, 100 mW/cm^2) activation.

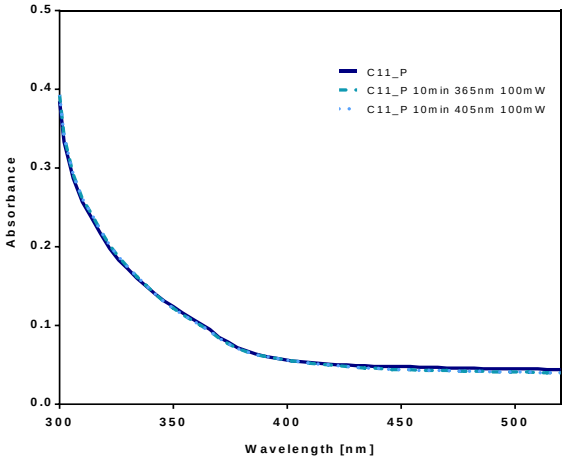

Figure 26. UV/vis spectrum of C11_P nanoparticles (200 µg/mL) supernatant before and after UV (365 nm, 10 minutes, 100 mW/cm^2) and blue laser (405 nm, 10 minutes, 100 mW/cm^2) activation.

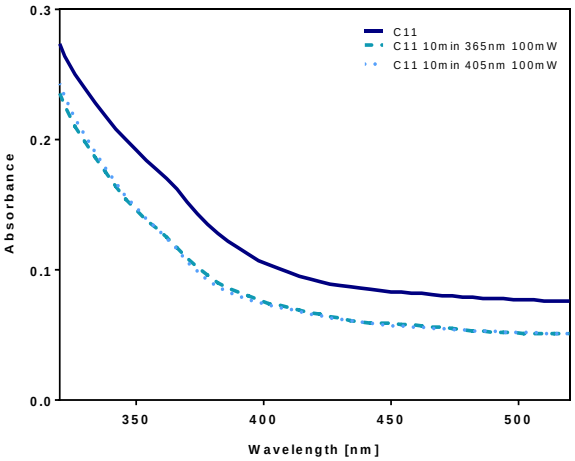

Figure 27. UV/vis spectra of a suspension of C11 nanoparticles (200 µg/mL) before and after UV (365 nm, 10 minutes, 100 mW/cm^2) or blue laser (405 nm, 10 minutes, 100 mW/cm^2) activation.

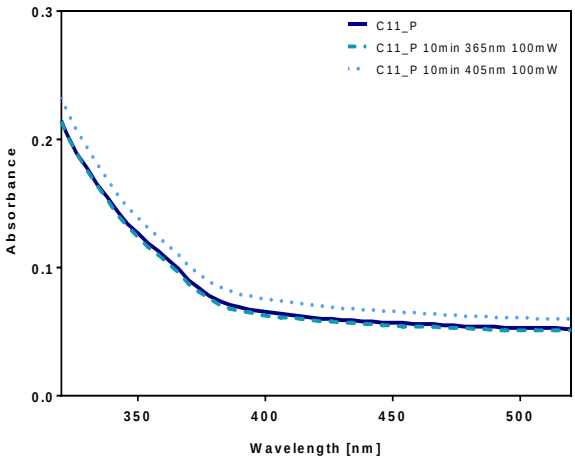

Figure 28. UV/vis spectra of a suspension of C11_P nanoparticles (200 µg/mL) before and after UV (365 nm, 10 minutes, 100 mW/cm^2) or blue laser (405 nm, 10 minutes, 100 mW/cm^2) activation.

For C11 nanoparticles supernatant (Figure 25), an increase in the absorption peak at 355 nm after light activation was observed. These results agree with the release of DMNC moieties from the C11 nanoparticles after photo-activation with both light sources (UV light and blue laser), as expected from the photo-cleavage mechanism. The decrease of signal in C11 resuspended nanoparticles after UV and blue laser exposure (Figure 27) indicates that DMNC concentration in nanoparticle decreases after light activation, confirming the light-triggered release of DMNC from nanoparticles. Overall, our results indicate that C11 nanoparticles respond efficiently to light activation.

Analysing both Figure 26 and Figure 28, there is no significant difference for supernatants and/or resuspended nanoparticles spectra, before and after photo-activation of C11_P nanoparticles. In resuspended nanoparticles exposed to blue laser (Figure 28) a small shift through the spectrum is observed, but not specifically for any wavelength or peak. So, this shift is considered an artefact of the measurement and has no significance in the analysis of the present results. For C11_P nanoparticles we can conclude there's no light response from the nanosystem, neither to UV (365 nm) nor to blue laser (405 nm), since it was no possible to observe the DMNC moieties photo-cleavage and their consequent release to the supernatant.

Overall, UV/vis spectrophotometry measurements confirm DLS results. C11 nanoparticles are photo-responsive and light activation promotes the release of photo-cleavable moieties into the solution (supernatant). In addition, C11_P nanoparticles showed lower photo-responsiveness to blue laser stimuli as detected by DLS (C11_P nanoparticles: ~37% of count decrease after light activation, C11 nanoparticles: 80% of count decrease after light activation). For subsequent experiments, we have used C11 nanoparticles.

3. Cytotoxicity of nanoparticles

Previously, experiments with UV light were performed in the lab by Josephine Blersch using a transilluminator's Epi illumination at 365 nm (power intensity: 1 mW/cm^2). She has shown that cell viability was not compromised when cells were transfected with 20 µg/mL of C11 nanoparticles and exposed to UV light (365 nm) during 10 minutes (~100% cell viability). Under these conditions, it was also demonstrated the disassembly of the nanoparticles. The activation of the nanoparticles outside the UV range is more promising from a translational point of view and thus tested in the present thesis. In order to assess blue laser (405 nm) photo-cytotoxicity, HeLa-GFP cells were exposed to three different light intensities: 80 mW/cm^2, 20 mW/cm^2 and 10 mW/cm^2 at continuous radiation, for three different time intervals: 30 seconds, 1 minute and 3 minutes. Cell viability was measured by an automated fluorescence microscopy and analysed in the InCell Analyzer developer software. The results are presented in Figure 29.

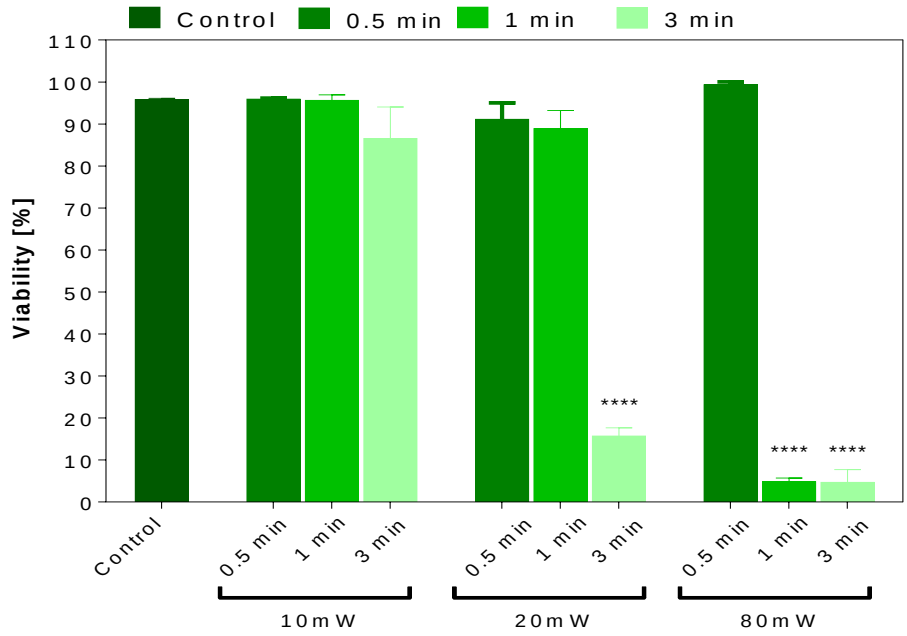

Figure 29. HeLa-GFP cells viability (%) after blue laser exposure. Cells were exposed to a blue laser (405 nm), at 80 mW/cm^2, 10 mW/cm^2 and 20 mW/cm^2, during 30 seconds, 1 minute and 3 minutes, and cultured for 48h. HeLa-GFP cells not exposed to the blue laser were used as control. Cells were stained with PI and H33342. The % of cells viability was evaluated by fluorescence microscopy (see Materials and Methods). Results are expressed as Mean±SEM (n=3, statistical significance: **** P < 0.0001).

Our results showed that cell viability didn't change significantly in the first 30 seconds, for all light intensities tested as compared to control (non-irradiated cells). However, cell viability is impaired after cell exposure to a laser of 20 mW/cm^2 or 80 mW/cm^2 for times above 3 minutes or 1 minute, respectively. On the other hand, when laser power is 10 mW/cm^2 cell viability is not significantly affected for all the exposure times tested (~>90% cell viability), and so happens for 30 seconds and 1 minute when 20 mW/cm^2 laser power is used. Overall, our results indicate that the blue laser has cytotoxicity for high power values and times. 10 mW/cm^2 is by far the best condition tested, since it didn't affect cells viability after exposure for any of the time intervals tested. Thus, for further experiments, blue laser (405 nm) at 10 and 20 mW/cm^2 will be used.

Next, C11 nanoparticles were complexed with siRNA against GFP and CY5-labelled siRNA, with a complexation efficiency above 80%. Cells were then transfected with C11@siRNA complexes (20 µg/mL of nanoparticles) during 10 minutes. After transfection, cells were irradiated with a blue laser (405 nm, continuous radiation), at different powers (10 and 20 mW/cm^2), and during different times (30 seconds, 1 minute and 3 minutes). Forty-eight hours after transfection, cell images were obtained by an automated fluorescence microscopy and analysed in the InCell Analyzer developer software. Analysis assessed the nanoparticles cytotoxicity (by cell viability), siRNA internalization and the intracellular siRNA release mediated by photo-activatable nanoparticles (by GFP knockdown).

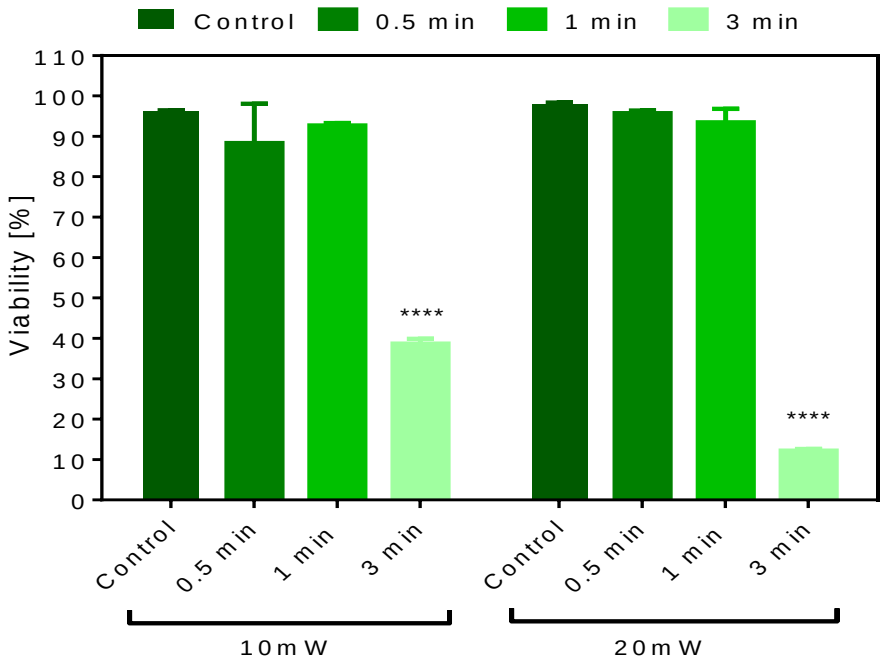

Figure 30. Effect of C11 nanoparticles in HeLa-GFP cells viability (%) after blue laser exposure. Cells were transfected with C11 nanoparticles complexed with siRNA (20 µg/mL) before light activation. Photo-activation was performed using a blue laser (405 nm at 10 mW/cm^2 and 20 mW/cm^2), during 30 seconds, 1 minute and 3 minutes. HeLa-GFP cells transfected with C11-NP but not exposed to a blue laser were used as control. Cells were stained with PI and H33342 and the % of cells viability was evaluated by fluorescence microscopy, 48h after transfection (see Materials and Methods). For each condition tested, there were performed three technical replicates. Results are expressed as Mean±SEM (n=3, statistical significance: **** $P < 0.0001$).

Cells viability is above 80% after transfection with 20 µg/mL of C11 nanoparticles and also after photo-activation with a blue laser at 10 mW/cm^2 or 20 mW/cm^2, during 30 seconds and 1 minute. However, viability decreases significantly after photo-activation using 20 mW/cm^2 during 3 minutes (~5% cells viability), and gets compromised also for this time interval when irradiation power is 10 mW/cm^2. Results are similar to the ones obtained in photo-cytotoxicity assays (see previous section), indicating that the cytotoxicity verified in the present results is mainly an effect from the light while C11 nanoparticles are not significant toxic for cells at 20 µg/mL concentration. In addition, we can also assert DMNC photo-cleavage by-products are relatively non-cytotoxic [97]. Further experiments using the same light conditions were performed and corresponding results confirm the ones presented here (see supplementary material, Figure 34).

4. Intracellular siRNA release mediated by photo-activatable nanoparticles

In order to assess siRNA intracellular release mediated by C11 nanoparticles, GFP knockdown in transfected HeLa-GFP cells was determined. Similarly to previous experiments, C11 nanoparticles were initially complexed with siRNA GFP Duplex I and siRNA labelled with CY5. HeLa-GFP cells were seeded 12-24h prior to experiment and then transfected with C11

nanoparticles complexed with siRNA (20 µg/mL of C11 nanoparticles) for 10 minutes, before irradiation. Then, UV (365 nm) and blue laser (405 nm) activation (continuous radiation) was done for 30 seconds, 1 and 3 minutes. Cells were stained and analysed by fluorescence microscopy 48h after cells transfection in InCell Analyzer equipment. GFP knockdown after UV light and blue laser exposure are presented below in Figure 31 and Figure 32, respectively. Representative images showing GFP knockdown after light irradiation can be found in supplementary material, Figure 37.

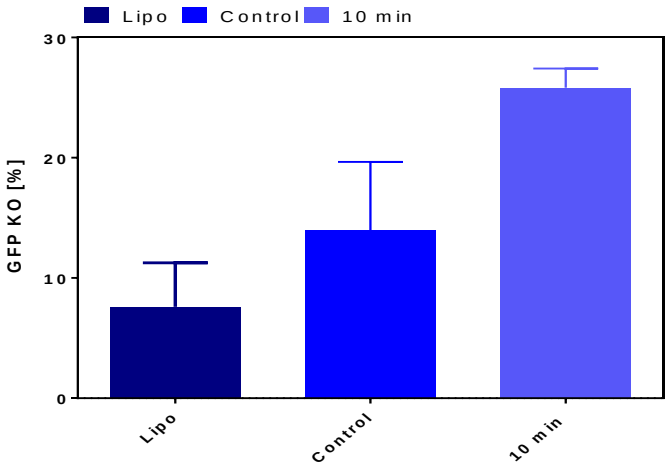

Figure 31. Intracellular siRNA release mediated by photo-activatable C11 nanoparticles – GFP KO (%) - after UV exposure. Cells were transfected with 20 µg/mL of C11 nanoparticles (complexed with modified siRNA GFP Duplex I and siRNA labelled siRNA with CY5 stain) during 10 minutes. Cells were exposed to UV light (365 nm), and stained with a solution composed by live nucleus staining (H33342) and dead nucleus staining (PI). Results were obtained by fluorescence microscopy in InCell Analyzer 2200 equipment (see Materials and Methods). As control, non-photo-activated C11 nanoparticles were used. GFP KO triggered by photo-activated nanoparticles and GFP KO due to the use of the commercial transfection agent lipofectamine (Lipo) were also compared. Data for % of GFP KO were obtained by InCell developer software. For imaging, there were acquired four image fields per well, giving data from a representative area of each well. For each condition tested, three technical replicates have been collected. Results are expressed as Mean±SEM (n=3).

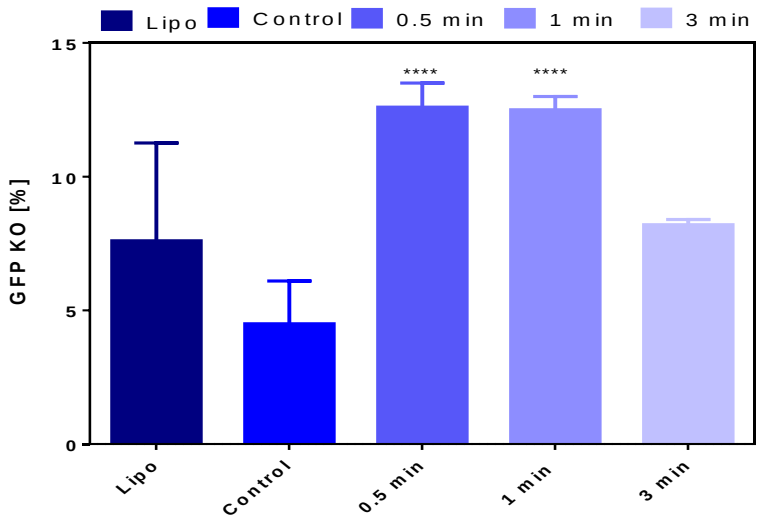

Figure 32. Intracellular siRNA release mediated by photo-activatable C11 nanoparticles – GFP KO (%) - after blue laser exposure, at 10 mW/cm^2. Cells were transfected with 20 µg/mL of C11 nanoparticles (complexed with modified siRNA GFP Duplex I and labelled siRNA with CY5 stain) during 10 minutes. Cells were exposed to laser (405 nm), and stained with a solution, composed by live nucleus staining (H33342) and dead nucleus staining (PI). Results were obtained by fluorescence microscopy in InCell Analyzer 2200 equipment (see Materials and Methods). As control, non-photo-activated C11 nanoparticles were used. GFP KO triggered by photo-activated nanoparticles and GFP KO due to the use of the commercial transfection agent lipofectamine (Lipo) were also compared. Data for % of GFP KO were obtained by InCell developer software. For each condition tested, three technical replicates have been collected. Results are expressed as Mean±SEM (n=3). Satistical significance: **** P < 0.00001, comparing to the control.

After UV light activation, there was a 2.5-fold increase in GFP knockdown (Figure 31). Similarly, after blue laser activation, there was a 2-fold increase in GFP knockdown (405 nm, 10 mW/cm^2, time: 30 seconds or 1 minute). Further experiments were performed using the same conditions for light activation by the blue laser and confirmed the results presented in here (see supplementary material, Figure 35 and Figure 36). These supplementary results reinforce the potential of blue laser to trigger siRNA release from photo-activatable C11 nanoparticles, particularly when exposed to 405 nm at 10 mW/cm^2 and during 30 seconds. Unfortunatelly, when irradiating using 20 mW/cm^2 power (see supplementary material, Figure 36), negative values after 30 seconds and 1 minute of light activation were obtained; and so, we can not conclude about siRNA release in these conditions. Importantly, GFP knockdown triggered by C11 nanoparticles photo-activation was generally higher than Lipofectamine (Lipo RNAiMAX®). Our results further show that the blue laser activation for 3 minutes is detrimental for GFP knockdown as compared to blue laser activation for 30 seconds or 1 minute. It is likely that low efficiency in knockdown is due to cell cytotoxicity demonstrated in previous section.

5.Conclusions

In this work, a photo-activatable nanosystem for siRNA delivery was developed, using polyplexes that were formed by a poly (amido amine)-based polymer bearing a pendant photo-cleavable moiety, DMNC. Photo-activatable nanoparticles (C11 nanoparticles) were produced by nanoprecipitation. Specifically, two formulations have been developed: one coming from the non-purified polymer, C11; and another one obtained from C11_P, the resulting polymer after purification of C11 by dialysis. The prepared nanoparticles showed interesting characteristics in terms of size (< 200 nm for C11 nanoparticles and < 100 nm for C11_P nanoparticles) and zeta potential (> 22 mV for C11 and > 15 mV for C11_P nanoparticles). The positive values for zeta potential are due to the presence of amine groups from the polymer in the nanoparticle structure. C11 nanoparticles (obtained from non-purified polymer) showed a much higher capacity to compensate siRNA negative charges after complexation. Complexation efficiency could be determined as > 80% by fluorescence spectroscopy.

The nanoparticles were responsive to UV (365 nm) and blue laser (405 nm). The analysis of % count decrease (> 80 % for C11 and ~37 % for C11_P nanoparticles) clearly showed that both nanoparticles respond to UV light. However, the nanoparticles more responsive to light are the ones obtained from the non-purified polymer as demonstrated by DLS and UV/Vis studies.

Our results further showed that light might be cytotoxic depending on its power and duration. We demonstrated that a blue laser of 80 mW/cm^2 might present high cytotoxicity after one minute of exposure. However, a blue laser of 10 mW/cm^2 had no significant effect on cell viability after 3 minutes of exposure. More importantly, cell viability was not affected by C11 nanoparticles (up to concentrations of 20 µg/mL), before or after light activation.

C11 nanoparticles are more efficient in the delivery of siRNA than lipofectamine under the conditions tested. A 2.5-fold increase in GFP knockdown was observed for cells transfected with C11 nanoparticles followed by UV activation as compared to cells not exposed to UV light.

4. Future perspectives

More studies need to be performed to study the knockdown mechanism induced by C11 nanoparticles. Further experiments to evaluate the activity of siRNA released after photo-activation may lead to better understanding of the formulation. These studies should be complemented by *in vitro* release studies of siRNA from the nanoparticle formulation. Additionally, it would be good to test different concentrations of nanoparticles (both higher and lower than 20 μg/mL) to exactly know which are the thresholds of both, nanoparticle cytotoxicity and minimum amount of nanoparticles to get a biological effect through siRNA release.

As previously mentioned, studies of internalization kinetics and assays to elucidate better the internalization pathways could be really important to understand and further develop nanosystems able to release siRNA in a more efficient way. siRNA has been selected as a model non-coding RNA in this study, but in future other ncRNAs such as miRNAs should be evaluated. Finally, *in vivo* tests should be performed using either siRNA or miRNA complexed to the light-responsive nanoparticles, in order to fully evaluate the potential of these release systems.

– This page was intentionally left blank –

5. References

1. Tiwari, G., et al. (2012). Drug delivery systems: An updated review. *International journal of pharmaceutical investigation, 2*(1), 2
2. Jain, K.K. (2014). *Drug delivery system*: Springer.
3. Timko, B.P., T. Dvir, and D.S. Kohane. (2010). Remotely triggerable drug delivery systems. *Adv Mater, 22*(44), 4925-43
4. Fatima, R., et al. (2015). Long noncoding RNAs in development and cancer: potential biomarkers and therapeutic targets. *Molecular and cellular therapies, 3*(1), 1
5. Zhang, Y. and R. Friedlander. (2011). Using non-coding small RNAs to develop therapies for Huntington's disease. *Gene therapy, 18*(12), 1139-1149
6. Gomes, A.Q., S. Nolasco, and H. Soares. (2013). Non-coding RNAs: multi-tasking molecules in the cell. *International journal of molecular sciences, 14*(8), 16010-16039
7. Carthew, R.W. and E.J. Sontheimer. (2009). Origins and mechanisms of miRNAs and siRNAs. *Cell, 136*(4), 642-655
8. Lam, J.K., et al. (2015). siRNA versus miRNA as therapeutics for gene silencing. *Molecular Therapy—Nucleic Acids, 4*(9), e252
9. Nayerossadat, N., T. Maedeh, and P.A. Ali. (2012). Viral and nonviral delivery systems for gene delivery. *Advanced biomedical research, 1*(1), 27
10. Uprichard, S.L. (2005). The therapeutic potential of RNA interference. *FEBS letters, 579*(26), 5996-6007
11. Blagbrough, I.S. and A.A. Metwally. (2013). *siRNA and Gene Formulation for Efficient Gene Therapy*: InTech.
12. Rayburn, E.R. and R. Zhang. (2008). Antisense, RNAi, and gene silencing strategies for therapy: mission possible or impossible? *Drug discovery today, 13*(11), 513-521
13. Desai, P.R., et al. (2013). Topical delivery of anti-TNFα siRNA and capsaicin via novel lipid-polymer hybrid nanoparticles efficiently inhibits skin inflammation in vivo. *Journal of Controlled Release, 170*(1), 51-63
14. Kumarswamy, R. and T. Thum. (2013). Non-coding RNAs in cardiac remodeling and heart failure. *Circulation research, 113*(6), 676-689
15. Tordonato, C., P.P. Di Fiore, and F. Nicassio. (2015). The role of non-coding RNAs in the regulation of stem cells and progenitors in the normal mammary gland and in breast tumors. *Frontiers in genetics, 6*
16. Zhou, J., et al. (2013). Nanoparticle-based delivery of RNAi therapeutics: progress and challenges. *Pharmaceuticals, 6*(1), 85-107
17. Singh, S., et al. (2011). Nanoparticle based drug delivery system: advantages and applications. *Indian Journal of Science and Technology, 4*(3), 177-180
18. Albanese, A., P.S. Tang, and W.C. Chan. (2012). The effect of nanoparticle size, shape, and surface chemistry on biological systems. *Annual review of biomedical engineering, 14*, 1-16
19. Singh, R. and J.W. Lillard. (2009). Nanoparticle-based targeted drug delivery. *Experimental and molecular pathology, 86*(3), 215-223
20. O'Mahony, A.M., et al. (2013). Non-Viral Nanosystems for Gene and Small Interfering RNA Delivery to the Central Nervous System: Formulating the Solution. *Journal of pharmaceutical sciences, 102*(10), 3469-3484
21. Mansour, H.M., Y.-S. Rhee, and X. Wu. (2009). Nanomedicine in pulmonary delivery. *Int J Nanomedicine, 4*, 299-319
22. Gimsa, J., P. Eppmann, and B. Prüger. (1997). Introducing phase analysis light scattering for dielectric characterization: measurement of traveling-wave pumping. *Biophysical journal, 73*(6), 3309

23. Varshosaz, J. and M. Farzan. (2015). Nanoparticles for targeted delivery of therapeutics and small interfering RNAs in hepatocellular carcinoma. *World journal of gastroenterology, 21*(42), 12022
24. Jesus, M. and V. Grazu. (2012). *Nanobiotechnology: inorganic nanoparticles vs organic nanoparticles* (Vol. 4): Elsevier.
25. Tang, L. and J. Cheng. (2013). Nonporous silica nanoparticles for nanomedicine application. *Nano today, 8*(3), 290-312
26. Ojea-Jimenez, I., et al. (2013). Engineered inorganic nanoparticles for drug delivery applications. *Current drug metabolism, 14*(5), 518-530
27. Bamrungsap, S., et al. (2012). Nanotechnology in therapeutics: a focus on nanoparticles as a drug delivery system. *Nanomedicine, 7*(8), 1253-1271
28. Mitragotri, S. and P. Stayton. (2014). Organic nanoparticles for drug delivery and imaging. *MRS Bulletin, 39*(03), 219-223
29. Lee, Y.S. (2011). *Self-assembly and nanotechnology systems: design, characterization, and applications*: John Wiley & Sons.
30. Cheng, R., et al. (2013). Dual and multi-stimuli responsive polymeric nanoparticles for programmed site-specific drug delivery. *Biomaterials, 34*(14), 3647-3657
31. Li, H., W. Tong, and C. Gao. (2016). Photo-responsive polyethyleneimine microcapsules cross-linked by ortho-nitrobenzyl derivatives. *J Colloid Interface Sci, 463*, 22-8
32. Mura, S., J. Nicolas, and P. Couvreur. (2013). Stimuli-responsive nanocarriers for drug delivery. *Nat Mater, 12*(11), 991-1003
33. Kim, C.S., et al. (2013). Triggered Nanoparticles as Therapeutics. *Nano Today, 8*(4), 439-447
34. Lu, Y., W. Sun, and Z. Gu. (2014). Stimuli-responsive nanomaterials for therapeutic protein delivery. *J Control Release, 194*, 1-19
35. McCoy, C.P., et al. (2010). Triggered drug delivery from biomaterials. *Expert opinion on drug delivery, 7*(5), 605-616
36. Liu, J., et al. (2014). pH-sensitive nano-systems for drug delivery in cancer therapy. *Biotechnology advances, 32*(4), 693-710
37. Tomlinson, R., et al. (2003). Polyacetal-doxorubicin conjugates designed for pH-dependent degradation. *Bioconjugate chemistry, 14*(6), 1096-1106
38. Galic, V.L., et al. (2011). Paclitaxel poliglumex for ovarian cancer. *Expert opinion on investigational drugs, 20*(6), 813-821
39. Cheng, R., et al. (2011). Glutathione-responsive nano-vehicles as a promising platform for targeted intracellular drug and gene delivery. *Journal of controlled release, 152*(1), 2-12
40. Meng, F., W.E. Hennink, and Z. Zhong. (2009). Reduction-sensitive polymers and bioconjugates for biomedical applications. *Biomaterials, 30*(12), 2180-2198
41. Cheng, W., et al. (2014). Stimuli-responsive polymers for anti-cancer drug delivery. *Mater Sci Eng C Mater Biol Appl, 45*, 600-8
42. Liu, S., Y. Tong, and Y. Yang. (2005). Thermally sensitive micelles self-assembled from poly (N-isopropylacrylamide-co-N, N-dimethylacrylamide)-b-poly (D, L-lactide-co-glycolide) for controlled delivery of paclitaxel. *Molecular BioSystems, 1*(2), 158-165
43. Zhu, L. and V.P. Torchilin. (2013). Stimulus-responsive nanopreparations for tumor targeting. *Integrative Biology, 5*(1), 96-107
44. Kumar, S.R., et al. (2014). Hydrophilic polymer coated monodispersed Fe3O4 nanostructures and their cytotoxicity. *Materials Research Express, 1*(1), 015015
45. Chorny, M., et al. (2010). Targeting stents with local delivery of paclitaxel-loaded magnetic nanoparticles using uniform fields. *Proceedings of the National Academy of Sciences, 107*(18), 8346-8351

46. Wang, S., et al. (2010). Targeted nanoparticles enhanced flow electroporation of antisense oligonucleotides in leukemia cells. *Biosensors and Bioelectronics, 26*(2), 778-783
47. Pruitt, J.D. and W.G. Pitt. (2002). Sequestration and ultrasound-induced release of doxorubicin from stabilized Pluronic P105 micelles. *Drug Delivery, 9*(4), 253-258
48. Huang, Y., et al. (2014). Photo-responsive polymeric micelles. *Soft Matter, 10*(33), 6121-38
49. Shah, S., P.K. Sasmal, and K.B. Lee. (2014). Photo-triggerable Hydrogel-Nanoparticle Hybrid Scaffolds for Remotely Controlled Drug Delivery. *J Mater Chem B Mater Biol Med, 2*(44), 7685-7693
50. Lin, M., et al. (2015). Near-infrared Light Activated Delivery Platform for Cancer Therapy

Adv Colloid Interface Sci, 226(Pt B), 123-37
51. Barhoumi, A. and D.S. Kohane. (2015). Light-controlled nanoparticulate drug delivery systems. 393-413
52. Rwei, A.Y., W. Wang, and D.S. Kohane. (2015). Photoresponsive nanoparticles for drug delivery. *Nano Today, 10*(4), 451-467
53. Carregal-Romero, S., et al. (2012). NIR-light triggered delivery of macromolecules into the cytosol. *J Control Release, 159*(1), 120-7
54. Liu, G.-Y., et al. (2012). Near-infrared light-sensitive micelles for enhanced intracellular drug delivery. *Journal of Materials Chemistry, 22*(33), 16865
55. Timko, B.P., et al. (2014). Near-infrared-actuated devices for remotely controlled drug delivery. *Proc Natl Acad Sci U S A, 111*(4), 1349-54
56. Luo, Y.-L., Y.-S. Shiao, and Y.-F. Huang. (2011). Release of photoactivatable drugs from plasmonic nanoparticles for targeted cancer therapy. *ACS nano, 5*(10), 7796-7804
57. Cho, H.J., M. Chung, and M.S. Shim. (2015). Engineered photo-responsive materials for near-infrared-triggered drug delivery. *Journal of Industrial and Engineering Chemistry, 31*, 15-25
58. Goodwin, A.P., et al. (2005). Synthetic micelle sensitive to IR light via a two-photon process. *Journal of the American Chemical Society, 127*(28), 9952-9953
59. Babin, J., et al. (2009). A New Two-Photon-Sensitive Block Copolymer Nanocarrier. *Angewandte Chemie International Edition, 48*(18), 3329-3332
60. Fomina, N., J. Sankaranarayanan, and A. Almutairi. (2012). Photochemical mechanisms of light-triggered release from nanocarriers. *Adv Drug Deliv Rev, 64*(11), 1005-20
61. Szymański, W., et al. (2013). Reversible photocontrol of biological systems by the incorporation of molecular photoswitches. *Chemical reviews, 113*(8), 6114-6178
62. Merino, E. and M. Ribagorda. (2012). Control over molecular motion using the cis–trans photoisomerization of the azo group. *Beilstein journal of organic chemistry, 8*(1), 1071-1090
63. Brieke, C., et al. (2012). Light-controlled tools. *Angewandte Chemie International Edition, 51*(34), 8446-8476
64. Bisby, R.H., C. Mead, and C.G. Morgan. (2000). Active Uptake of Drugs into Photosensitive Liposomes and Rapid Release on UV Photolysis¶. *Photochemistry and photobiology, 72*(1), 57-61
65. Barhoumi, A., Q. Liu, and D.S. Kohane. (2015). Ultraviolet light-mediated drug delivery: Principles, applications, and challenges. *J Control Release, 219*, 31-42
66. Wang, G., X. Tong, and Y. Zhao. (2004). Preparation of azobenzene-containing amphiphilic diblock copolymers for light-responsive micellar aggregates. *Macromolecules, 37*(24), 8911-8917
67. Tong, X., et al. (2005). How can azobenzene block copolymer vesicles be dissociated and reformed by light? *The Journal of Physical Chemistry B, 109*(43), 20281-20287

68. Katz, J.S. and J.A. Burdick. (2010). Light-responsive biomaterials: development and applications. *Macromol Biosci, 10*(4), 339-48
69. Zhao, H., et al. (2012). o-Nitrobenzyl alcohol derivatives: opportunities in polymer and materials science. *Macromolecules, 45*(4), 1723-1736
70. Chandra, B., et al. (2006). Formulation of photocleavable liposomes and the mechanism of their content release. *Organic & biomolecular chemistry, 4*(9), 1730-1740
71. Jiang, J., X. Tong, and Y. Zhao. (2005). A new design for light-breakable polymer micelles. *Journal of the American Chemical Society, 127*(23), 8290-8291
72. Liu, G. and C.M. Dong. (2012). Photoresponsive poly(S-(o-nitrobenzyl)-L-cysteine)-b-PEO from a L-cysteine N-carboxyanhydride monomer: synthesis, self-assembly, and phototriggered drug release. *Biomacromolecules, 13*(5), 1573-83
73. Wittrup, A., et al. (2015). Visualizing lipid-formulated siRNA release from endosomes and target gene knockdown. *Nature biotechnology, 33*(8), 870-876
74. Gilleron, J., et al. (2013). Image-based analysis of lipid nanoparticle-mediated siRNA delivery, intracellular trafficking and endosomal escape. *Nature biotechnology, 31*(7), 638-646
75. Sahay, G., et al. (2013). Efficiency of siRNA delivery by lipid nanoparticles is limited by endocytic recycling. *Nature biotechnology, 31*(7), 653-658
76. Wang, Y. and L. Huang. (2013). A window onto siRNA delivery. *Nature biotechnology, 31*(7), 611-612
77. Wang, J., et al. (2010). Delivery of siRNA therapeutics: barriers and carriers. *The AAPS journal, 12*(4), 492-503
78. Dominska, M. and D.M. Dykxhoorn. (2010). Breaking down the barriers: siRNA delivery and endosome escape. *J Cell Sci, 123*(8), 1183-1189
79. Whitehead, K.A., R. Langer, and D.G. Anderson. (2009). Knocking down barriers: advances in siRNA delivery. *Nature reviews Drug discovery, 8*(2), 129-138
80. Liang, W. and J.K. Lam. (2012). *Endosomal escape pathways for non-viral nucleic acid delivery systems*: INTECH Open Access Publisher.
81. Montier, T., et al. (2008). Progress in cationic lipid-mediated gene transfection: a series of bio-inspired lipids as an example. *Current Gene Therapy, 8*(5), 296-312
82. Malone, R.W., P.L. Felgner, and I.M. Verma. (1989). Cationic liposome-mediated RNA transfection. *Proceedings of the National Academy of Sciences, 86*(16), 6077-6081
83. Dalby, B., et al. (2004). Advanced transfection with Lipofectamine 2000 reagent: primary neurons, siRNA, and high-throughput applications. *Methods, 33*(2), 95-103
84. Spagnou, S., A.D. Miller, and M. Keller. (2004). Lipidic carriers of siRNA: differences in the formulation, cellular uptake, and delivery with plasmid DNA. *Biochemistry, 43*(42), 13348-13356
85. Schaffert, D. and E. Wagner. (2008). Gene therapy progress and prospects: synthetic polymer-based systems. *Gene therapy, 15*(16), 1131-1138
86. Vicennati, P., et al. (2008). Polyethylenimine in medicinal chemistry. *Current medicinal chemistry, 15*(27), 2826-2839
87. Anderson, D.G., et al. (2005). Structure/property studies of polymeric gene delivery using a library of poly (β-amino esters). *Molecular Therapy, 11*(3), 426-434
88. Deng, X., et al. (2014). Trigger-responsive, fast-degradable poly(beta-amino ester)s for enhanced DNA unpackaging and reduced toxicity. *Biomaterials, 35*(18), 5006-15
89. Dvir, T., et al. (2009). Photo-targeted nanoparticles. *Nano letters, 10*(1), 250-254

SUPPLEMENTARY MATERIAL

Appendix A

A.1 Cells counting method

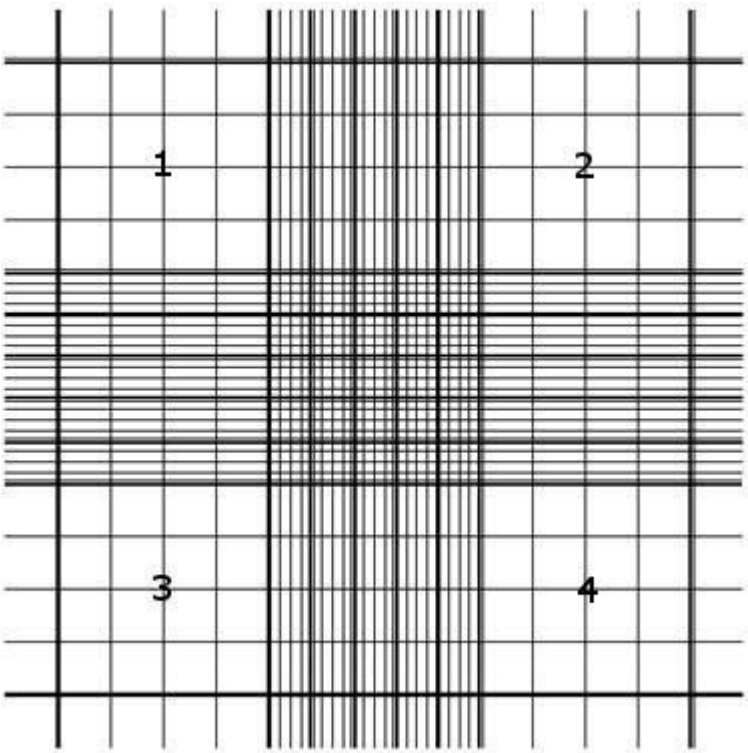

Figure 33. Neubauer Chamber Cells Counting. For each compartment Neubauer chamber, the cells were counted in the numbered squares (1, 2, 3 and 4). The total number of cells counted in each bin is the average of counted cells in four squares. At the end was made the average of counted cells in both compartments.

Appendix B

B.1 Photo-activatable nanoparticles cytotoxicity

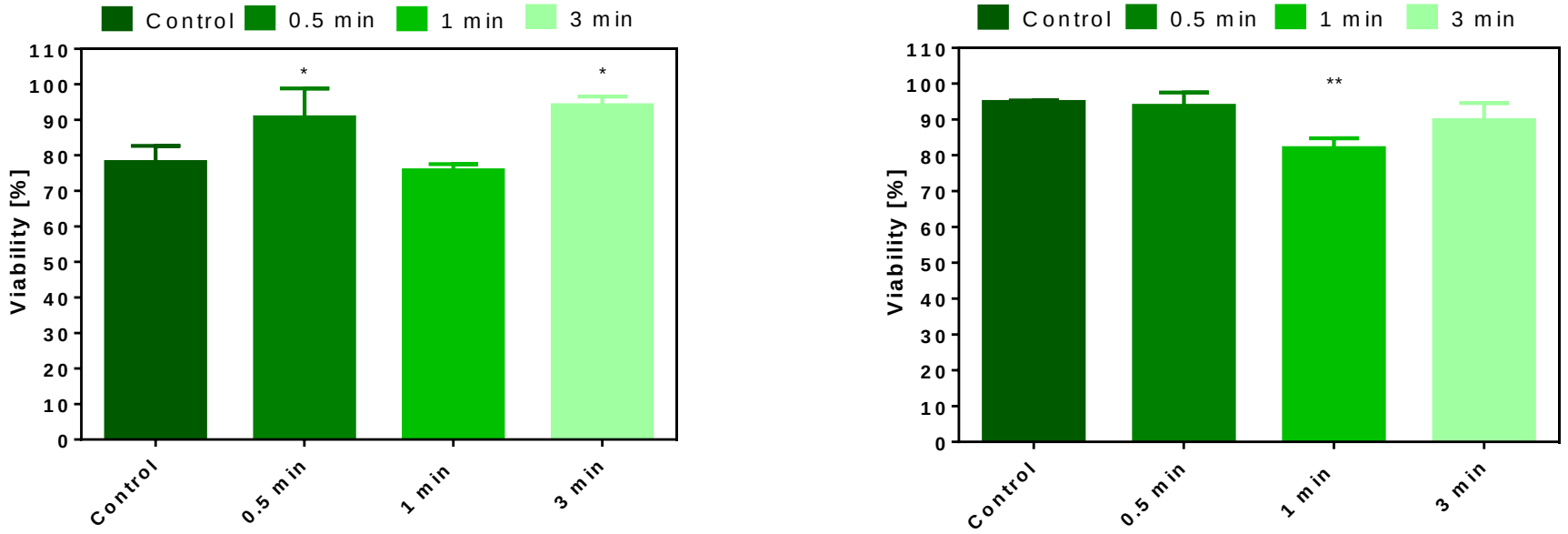

Figure 34. Effect of C11 nanoparticles in HeLa-GFP cells viability (%) after blue laser exposure. Cells were transfected with 20 µg/mL of C11 nanoparticles complexed with siRNA before light activation. Photo-activation was performed using blue laser (405 nm at 10 mW/cm^2), during 30 seconds, 1 minute and 3 minutes. HeLa-GFP cells but not exposed to the blue laser were used as control. Cells were stained with PI and H33342 and the % of cells viability was evaluated by fluorescence microscopy, 48h after transfection. For each condition tested, there were performed three technical replicates. Results are expressed in Mean±SEM (n=3, statistical significance: * $P \leq 0.05$, ** $P \leq 0.001$).

Appendix C

C.1 Intracellular siRNA release mediated by photo-activatable nanoparticles

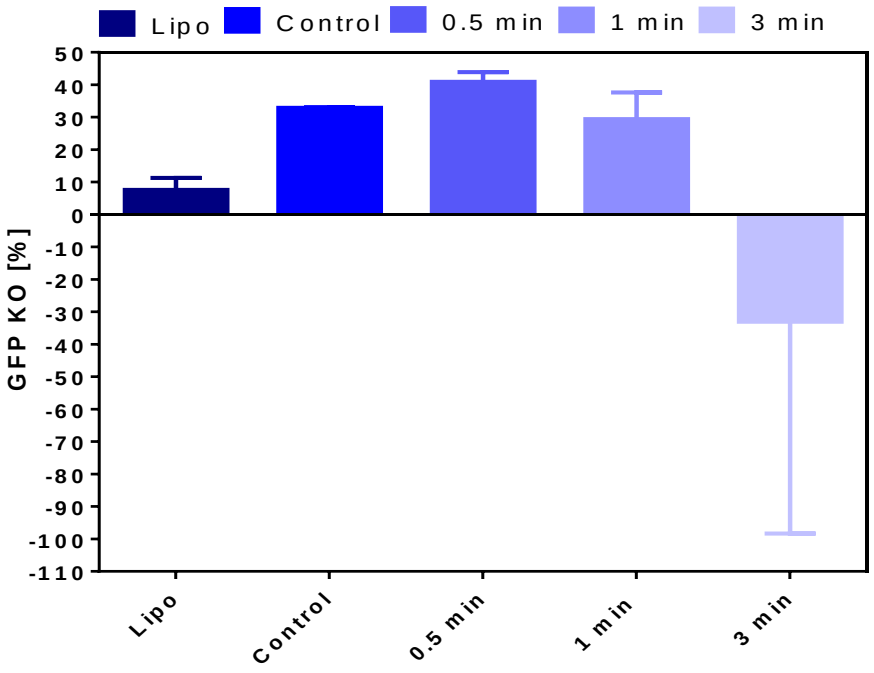

Figure 35. Intracellular siRNA release mediated by photo-activatable C11 nanoparticles – GFP KO (%) - after blue laser exposure, at 10 mW/cm^2. Cells were transfected with 20 µg/mL of C11 nanoparticles (complexed with siRNA GFP Duplex I and labelled siRNA with CY5 stain), during 10 minutes. Cells were exposed to laser light (405 nm) during 30 seconds, 1 minute and 3 minutes, and stained with a solution, composed by live nucleus staininge (H33342) and dead nucleus staining (PI). Results were obtained by fluorescence microscopy in InCell Analyzer 2200 equipment. Non-photo-activated C11 nanoparticles were used as control. GFP KO triggered by photo-activated nanoparticles and GFP KO due to the use of the commercial transfection agent lipofectamine (Lipo) were also compared. Data for % of GFP KO were obtained by InCell Analyzer developer software. For each condition tested, there were performed three technical replicates. Results are expressed in Mean of value±SEM (n=3).

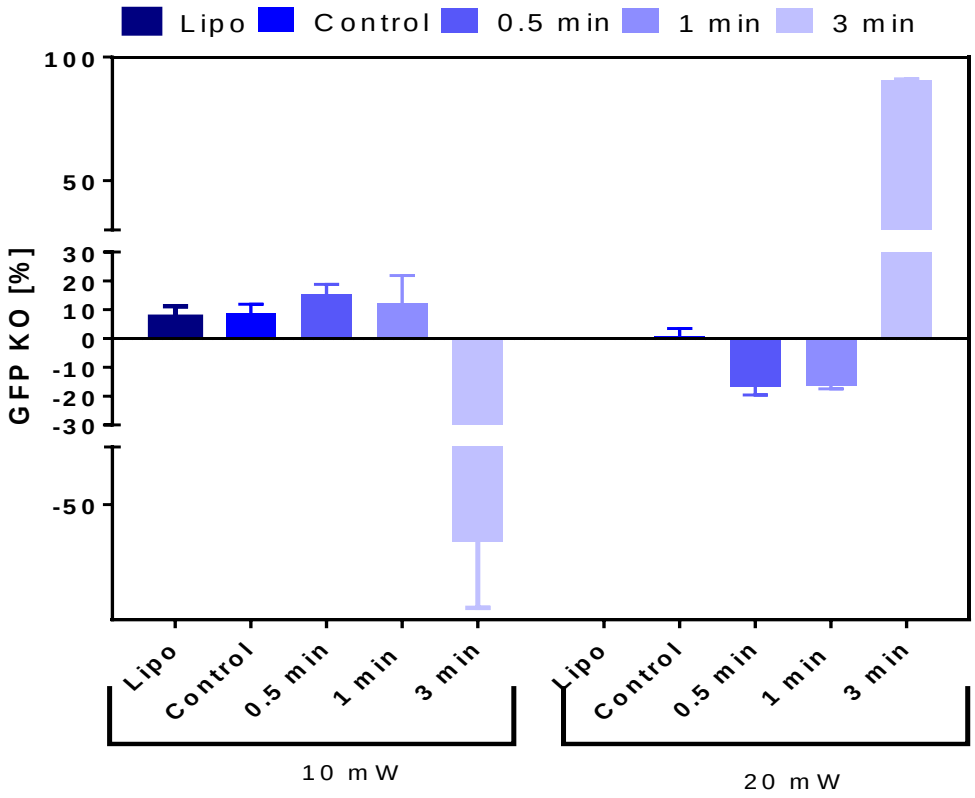

Figure 36. Intracellular siRNA release mediated by photo-activatable C11 nanoparticles – GFP KO (%) - after blue laser exposure, at 10 and 20 mW/cm^2. Cells were transfected with 20 µg/mL of C11 nanoparticles (complexed with siRNA GFP Duplex I and labelled siRNA with CY5 stain), during 10 minutes. Cells were exposed to laser light (405 nm), and stained with a solution, composed by live nucleus staining (H33342) and dead nucleus staining (PI). Results were obtained by fluorescence microscopy in InCell Analyzer 2200 equipment. Non-photo-activated C11 nanoparticles were used as control. GFP KO triggered by photo-activated nanoparticles and GFP KO due to the use of the commercial transfection agent lipofectamine (Lipo) were also compared. Data for % of GFP KO were obtained by InCell Analyzer developer software. For each condition tested, there were performed three technical replicates. Results are expressed in Mean of value±SEM (n=3).

Appendix D

D.1 Images from HeLa-GFP cells, highlighting cells viability and GFP knockdown

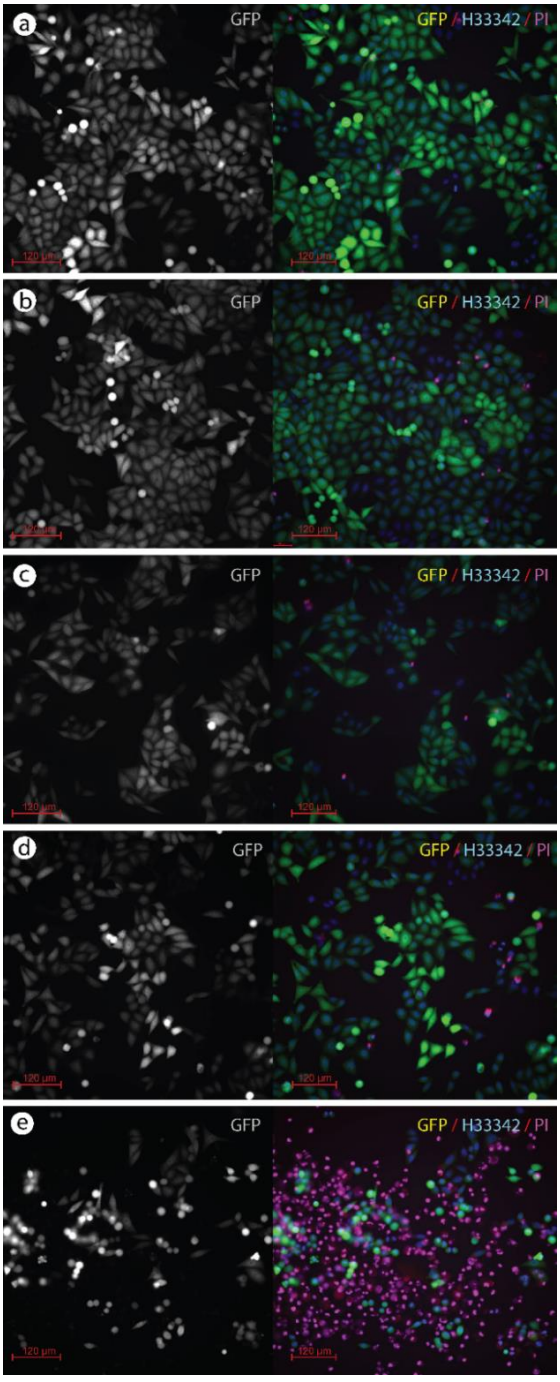

Figure 37. Representative images to section 3.1.1. from *In Vitro* studies and Figures 30 and 32. Monochrome GFP left picture and merge of FITC (GFP, green color), DAPI (H33342, blue nucleus) and CY3 (PI, red nucleus) channel, right picture. a): HeLa-GFP cells without nanoparticles and without light irradiation; b): Cells transfected with C11 nanoparticles without light irradiation; c) Cells transfected with C11 nanoparticles, after laser irradiation (405nm, 10 mW/cm^2, during 30 seconds); d) Cells transfected with C11 nanoparticles, after laser irradiation (405nm, 10 mW/cm^2, during 1 minute); e) Cells transfected with C11 nanoparticles, after laser irradiation (405nm, 10 mW/cm^2, during 3 minutes).